Studies of Primary Electron Sources

W. G. SHEPHERD, Chief Investigator
Report Prepared by D. E. ANDERSON

ELECTRON TUBE RESEARCH LABORATORY
UNIVERSITY OF MINNESOTA
INSTITUTE OF TECHNOLOGY

Contract No. AF 19(604)-8381
Project 4619
Task 46190

Scientific Report No. 6
June 1, 1962 to September 1, 1962
January 1963

Prepared for

ELECTRONICS RESEARCH DIRECTORATE
AIR FORCE CAMBRIDGE RESEARCH LABORATORIES
OFFICE OF AEROSPACE RESEARCH
UNITED STATES AIR FORCE
BEDFORD, MASSACHUSETTS

Requests for additional copies by Agencies of the Department of Defense, their contractors, and other Government agencies should be directed to the:

ARMED SERVICES TECHNICAL INFORMATION AGENCY
ARLINGTON HALL STATION
ARLINGTON 12, VIRGINIA

Department of Defense contractors must be established for ASTIA services or have their "need-to-know" certified by the cognizant military agency of their project or contract.

All other persons and organizations should apply to the:

U.S. DEPARTMENT OF COMMERCE
OFFICE OF TECHNICAL SERVICES
WASHINGTON 25, D. C.

Table of Contents

I. Abstract

A tube structure designed to expose an oxide cathode to a controlled partial pressure of an alkaline-earth metal vapor is described and results obtained from the first tube are presented.

Photoelectric yield measurements are presented which illustrate the effect of the environment on the yield from a BaO coating. The system used for the simultaneous determination of the photoelectric and thermionic emission energy distributions from BaO is presented and described in detail. Measurements of the thermionic emission energy distribution are presented and these distributions are used in an evaluation of the analyzer system. Thermionic energy distributions are presented which provide evidence for a coating potential drop while drawing dc current from the coating and a measure of the potential profile of the coating is derived from these distributions.

Results of a further study of the dependence of thermionic pulse emission, conductivity, and Sr evolution on the oxide thickness are presented for a tube which operated for only a limited time. No clear-cut dependence on coating thickness was observed.

Methods of formation of insulating films for thin film tunnel current devices are discussed. Al_2O_3 was anodically formed using four electrolytic solutions, and 4 types of heat treatment were used. Preliminary results from these samples are presented, which show that the electrical properties of the insulating films are quite insensitive to the anodizing techniques used.

Electron emission into vacuum from Al-Al_2O_3-Au thin film sandwich devices is described. The emission currents observed are

stable and reproducible within the limits imposed by the aging and hysteresis effects exhibited by the sample currents. Preliminary measurements of the current transfer ratio are presented for various Au overlayer thicknesses.

A study of arc formation above a liquid gallium pool cathode is described. A stable arc discharge above such a low vapor pressure liquid would permit electron extraction into a high vacuum system. It was found to be not possible to ignite and maintain an arc from the gallium pool at reasonable current and voltage levels. Possible applications of a gallium pool switch, capable of opening cleanly at high voltage while carrying high currents, are discussed.

II. Studies of Thermionic Cathodes

1. Introduction

The studies to be reported in this section are all directed to obtaining an understanding of the alkaline-earth metal oxides as thermionic cathodes. While other systems will be investigated later, it is felt that the present understanding of the oxide cathode is such as to make specific studies of this system most fruitful at the start.

The purpose of this introduction then is to review the groundwork on which these researches are based, to summarize briefly the important results of our previous work,* and to present the general outline of the plan by which the particular objectives of the research are being approached. We hope that such a resume will serve to relate the individual experiments to the program as a whole.

There is general agreement that the oxide cathode is an n-type semiconductor and that an excess of alkaline-earth metal in the coating is essential for high emission. It is not necessary to assume that this excess metal must occur in the grains of the coating in order to provide donors, but only that the presence of free metal in the pores is necessary for the production of donors. This excess metal is believed to result largely from the action of reducing impurities incorporated in the base nickel. It might reasonably be expected that the evaporation

* Bureau of Ships, Contract NObsr-63172, Air Force Cambridge Research Laboratories, Contract No. AF 19(604)-3890.

rate of free alkaline-earth metal from the oxide coating would serve as an indication of the rate at which this free metal is being produced by chemical reduction. Thus, the evaporation rates of such free metal might be correlated with the emission capabilities of the cathode.

As a convenient and accurate means for measuring the rate at which the alkaline-earth metal is evolved from the coating, radioactive tracers of Ba or Sr can be incorporated in the oxide coating. This method allows one to monitor the total amount of alkaline-earth metal being evolved from the coating, either as the oxide or as the free metal. Although the total amount of Ba evaporated (Ba and BaO) is larger than that of Sr (Sr and SrO), our observation is that the metal-to-oxide ratio is more favorable for the detection of Sr metal than for Ba metal in the presence of the background of oxide evaporation.

Subsequent experiments were designed to determine whether a correlation existed between the Sr evaporation and the emission from oxide-coated cathodes. For these experiments cathodes based on single additive nickel alloys and on pure nickel doped with carbon have been used. A correlation between Sr evaporation and the development of emission has been observed for both types of cathode base. This correlation has been qualitatively explained using a model in which the strontium evolution follows the rate at which the reducing agent arrives by diffusion at the base nickel-oxide interface. The emission is taken as being controlled by the donor concentration in the oxide particles,

with the generation of additional donors at the surface of each particle being a function of the pressure of free alkaline-earth metal in the pores of the coating.

It has been found that, for the concentrations studied, single additive alloys of Al, Mn, W, Mg, and Si and Ni lead to a rate of coating reduction which is limited by the diffusion of the reducing element to the oxide coating-base metal interface. In these cases the rate of reduction is proportional to $t^{-1/2}$ where t is the total operating time. Quantitative agreement with observed data can be obtained when the diffusion coefficient of each additive in nickel is known; these values have been determined. Early studies of the pulse emission from cathodes based on these alloys indicated that, following an initial activation, the emission declined monotonically with cathode life. It is postulated that this decline is a consequence of competing processes and that, under ideal conditions, stable emission levels should be maintained even for the systems with declining rates of chemical reduction. This "stable donor" behavior has been observed with cathodes based on Mg-Ni and Al-Ni alloys.

It is possible to devise a cathode base from which carbon can be dispensed to the coating at a rate which is constant over extended periods of time. The Sr evolution from coatings based on such a dispenser is found to be constant. This system is of considerable interest because of the possibility of producing chemical reduction of the coating at a constant and controllable rate.

All of the foregoing studies have been made with the cathode in thermal equilibrium at a fixed temperature. A complete understanding of the factors affecting chemical activation demands information as to their temperature dependence. An experimental investigation of the response of oxide cathodes to step changes in temperature has been made which shows both short-term and long-term changes, corresponding respectively to (1) the fraction of the donors thermally ionized and (2) changes in the equilibrium concentration of donors.

Anode poisoning of an oxide cathode, caused by drawing current to an electrode which has accumulated evaporation products from the cathode, has been studied with respect to the change in activity during such poisoning and to subsequent recovery. The pulse emission under these conditions may drop from amps/cm^2 to milliamps/cm^2 with an apparent exponential decay having a time constant of a few minutes. It is known from other studies made in these laboratories that there is a low-voltage threshold for the dissociation of anode deposits or desorption of gas layers. If the anode bombardment is stopped when the emission has fallen to a stable level, the pulse emission then recovers in a manner very closely resembling the initial chemical activation of the cathode. It has been shown that the material which dissociates under electron bombardment is an impurity, rather than the oxides, related to the bakeout of the envelope of the structure.

It has also been found that the "long-pulse transients" which occur during heavy pulse current drain depend on the anode material and its past history. When an anode is used which has not been suitably processed a decay characterized by a 100 μsec time constant occurs, similar to that described by Sproull, and by Matheson and Nergaard. When a Ti anode which has been suitably processed is used the emission decay no longer occurs, and instead an emission enhancement is observed. This enhancement has shown to be consistent with a model in which thermal processes are invoked and which appears to describe correctly the thermal runaway which leads to cathode sparking.

Two major processes can contribute to the activation of the oxide cathode. These are chemical activation due to reducing agents incorporated in the base metal and electrolytic activation of the coating. The effect of chemical activation has been studied by operating the cathodes without current drain during life. Early attempts to produce simple electrolytic activation by drawing a continuous current from an oxide cathode based on a passive nickel led to activity levels which were much lower than could be achieved from cathodes based on active nickels in which chemical activation played a role. The results of studies of bombardment-induced poisoning suggested that this competing process limited the development of electrolytic activation. Accordingly, a structure was developed which permits the drawing of a continuous current to a positive grid located so close to the cathode that the threshold for anode poisoning would not be exceeded. Under these conditions,

a very pronounced activation of the cathode occurred when continuous current was drawn through the coating. It was found that the cathode activated with a time constant of the order of 10 minutes at 1119°K, and also that a continuation of current drain for several hours resulted in the development of a stable level of activity which then persisted even when current drain was discontinued.

These results have been interpreted in terms of a model in which the donors are not volatile and are thus stable in the absence of competing processes. A continuous current drain leads to a field-enhanced preferential evolution of anions from the coating with a corresponding increase in donor concentration, and emission capability, at the surface of the individual oxide grains. The permanent activation is viewed as the result of a saturation of the bulk of the oxide particles by the presence of this excess donor concentration at the surface.

The apparent emission measured from an oxide cathode by a method dependent on the deviation from a three-halves power law is influenced by the resistive drop in the oxide coating. This drop can develop across a resistance appearing at the interface between the oxide coating and the base metal and also across a resistance occuring in the bulk oxide. Studies of the formation of resistive interface layers for various reducing impurities have shown that only in the case of silicon is a significant resistive interface layer developed. The bulk resistive effects can be compensated by suitable measuring instrumentation and thereby an accurate determination of the saturation pulse emission

and of the coating resistance can be made. The necessary instrumentation to permit this has been developed in this laboratory. The deviation of a plot of (i) vs (v-ki) is observed with k adjusted to fit a 3/2 power space-charge curve. As a measure of the saturation emission, either J_{20} (the current at which the I-V trace has fallen 20% below the space-charge law) or J_d (the current at which deviation begins) can be determined.

2. Controlled Activation and Deactivation of Oxide Cathodes

R. H. Springer

Results obtained from the chemical activation studies conducted at this laboratory indicate that an excess of alkaline-earth metal in a cathode operating without current drain will greatly enhance the saturated pulse emission. Data from the controlled chemical activation tubes, which incorporated carbon as a reducing agent in the Ni base, indicate that the pulsed emission is proportional to the square root of the Sr evolution rate, which is proportional to the free metal concentration in the pores of the cathode.

If the excess metal in the coating is the origin of the enhanced emission from the oxide cathode, and diffusion into the bulk from the vapor phase is the mechanism whereby it is introduced, it should be possible to introduce it into the coating in a more controllable manner by means other than chemical reduction of the coating. A series of experiments were performed under a previous contract in which the Ba vapor pressure in the tube was controlled by placing the entire tube in an oven. The results from this study*

*Scientific Report No. 9, Studies on Base Nickels for Oxide-Coated Cathodes, Contract No. AF 19(604)-3890, pp. 22-35.

conflicted with the carbon study mentioned previously. These results are not clear-cut because of the possibility of a poisoning agent being evolved from the hot glass walls with a temperature dependence similar to that of the Ba source.

In an effort to determine the origin of these differences a tube structure was designed in which a large heatable Ti anode, with a heavy layer of the alkaline-earth metal, can be moved over the cathode. It is argued that if this anode is large enough it approximates, as far as the cathode is concerned, a system with all the walls being at anode temperature. This is not exactly true, of course, but this system removes the serious objection of having very warm glass present during the experiment and allows the anode material to be heated over the cathode, before the alkaline-earth metal is added, to determine the anode effect on the pulse emission.

The tube structure is shown in Fig. 1. The oxide cathode is situated in a heat shield assembly to which are attached two small swinging Ti anodes, one used during life periods and the other for pulse emission measurements. A large heatable Ti anode is positioned to that it can swing over either the evaporator or the cathode. The temperature of the anode is measured by a Pt - Pt 10% Rh thermocouple. This anode is supported by a large Ta disc bearing with thermocouple leads, and leads to the heaters in the anodes brought out on loosely coiled Pt leads.

The evaporator consists of a Ti cone which is heated from below by electron bombardment from a hot W filament. The evaporator is loaded with the appropriate carbonate, mixed with Ti chips and

converted to the oxide by heating in a vacuum. When the oxide is heated, it is reduced by the Ti and evolves the free alkaline-earth metal. This reaction is verified by observing the deposit on the tube wall with the anode moved to one side.

The first tube of this type QN1BB, was constructed and pre-processed. The tube was evacuated, baked and all the metal parts outgassed, without the oxide cathode or the reaction chemicals in the Ti cone.

The tube was then opened and a $(BaSr)CO_3$ coating on a pure Ni base, was inserted and the evaporator filled with $BaCO_3$ and Ti. The tube was then resealed, using argon as a flushing gas, and sealed to a Ti sputter pump station and pumped down. This structure was then baked for 12 hours at 400°C. After outgassing all metal parts by rf induction heating the cathode was converted to the oxide following the standard heating schedule presented earlier.* After conversion the coating was not uniform and hence this cannot be considered as a "standard" cathode but the processing was continued to check out the functioning of different parts of the tube.

The evaporator was heated, with the anode moved to one side, and the $BaCO_3$ converted to BaO. The anode was then outgassed and the tube removed from the pump station and its associated sputter pump put in operation. The pressure at this stage was 10^{-9} Torr, although higher pressures were observed with the evaporator in operation.

*Scientific Report No. 2, Studies on Base Nickels for Oxide-Coated Cathodes, Contract No. AF 19(604)-3890.

The cathode was then heated to a brightness temperature of 780°C and pulsed to the large swinging anode. The data are shown in Fig. 2.

In the interval from 0 to t_1 hours the anode was left at ambient temperature, and moved in place only to pulse, to determine the background emission. From t_1 to t_2 the anode was heated to 320° C in a remote position, without any observable influence on the cathode emission. From t_2 to t_3 the anode was heated to 400°C directly over the cathode and small changes are observed. Then, at t_3, the anode was exposed to the evaporator for two hours keeping the tube pressure below 5×10^{-7} Torr during heating of the evaporator. The anode with the evaporated Ba layer was then placed over the heated cathode and left to operate from t_3 to t_4 at 100°C, without applying anode heater power. This temperature was increased to 150°C at t_4 and 175°C at t_5. There were no pronounced changes in the emission and it was postulated that there was insufficient free Ba on the anode. At t_6 the anode was placed over the evaporator with the cathode turned off, and the evaporator was operated for 6.5 hours keeping the tube pressure below 8.0×10^{-7} Torr.

The cathode temperature was held at 780°C while the anode temperature was set at 300°C. The pulse emission increased by an order of magnitude to 4.2 amps/cm^2. At t_7 the anode temperature was reduced to ambient and the emission decreased to the background level. At t_8 the anode temperature was increased to 250°C which resulted only in a very small increase in emission.

It is postulated that there was insufficient Ba coverage on the anode to yield an anode surface characterized by bulk Ba properties. As a result of inadvertently tipping the tube during seal-off and consequently losing a large fraction of the Ba source from the evaporator, it might not be possible to obtain the needed coverage. As a result of this, and the questionable condition of the cathode, measurements were discontinued. It was found that the evaporator functions properly and that the heatable anode system will be suitable for further studies.

Two new tubes of this type are now being constructed and it is planned to incorporate a Ba source in one and a Sr source in the other.

3. Optical Measurements of Oxide Cathodes

A. Total Photoelectric Yield from BaO. C. A. Stolte

The results described in previous reports indicate that the photoelectric yield and thermionic emission from BaO are very dependent upon the environment of the coating. Previous results demonstrated that the room-temperature photoelectric yield from BaO, following a life period at 800°C, decreases as a function of time. Further data has been obtained which indicate that the decrease is not a donor diffusion effect but rather the result of a competing process which reduces the donor population at the surface of the coating. These data were obtained using a BaO coating based on 0.024% MgNi which, together with new Ti anodes, was mounted in the liquid nitrogen structure shown in Fig. 3 of the last report. The tube was evacuated on a Ti sputter pump station and all metal parts RF'ed to 800°C. The

structure was baked at 450°C for 7 hours and all metal parts again RF'ed. The tube was then sealed from the station and mounted in a light-tight box with the Ti sputter pump on the tube operating to further reduce and maintain a low pressure in the tube.

The $BaCO_3$ coating was converted to BaO by increasing the cathode temperature to 800°C, holding the pressure below 2×10^{-5} Torr; the pulse emission at 800°C was less than 5 mA/cm^2. The temperature was then increased in steps of 25°C every two minutes up to 1050°C and then reduced to 800°C. The pulse emission at 800°C was 0.9 A/cm^2 after this conversion schedule. Liquid nitrogen was placed around the cathode press to quench the coating to a low temperature and the filament voltage reduced to zero.

The total photoelectric yield plot taken 29 minutes after the filament was shut off is shown as curve #1 of Fig. 3. This curve is similar, in magnitude and shape, to those obtained from cathode PL2FF1, shown in the last report. After curve #1 was obtained the yield at 2.5 eV was monitored while the coating temperature was increased by means of applying filament power, with the press remaining in liquid N_2. The results are plotted in Fig. 4 where the yield at 2.5 eV, η (2.5), the coating temperature in °K, and the pressure as measured by the Ti sputter pump are plotted vs. time in minutes. Increasing the cathode temperature to 356°K, with the liquid nitrogen around the press assembly, had very little effect on the yield. However, when the liquid nitrogen was removed the yield decreased rapidly while the pressure in the tube and the temperature of the cathode

increased. From these data it is evident that the decrease observed is not a donor diffusion process, which would be temperature dependent, but a competing process, a consequence of the increased pressure, which reduced the donor population. It should be noted that the peak pressure burst (measured at the remote sputter pump) was still only 2×10^{-9} Torr.

The cathode was allowed to remain at room temperature in the dark for 5.75 hours. The coating was again quenched to liquid nitrogen temperature and the yield curve #2 of Fig. 3 obtained. The curve taken with increasing photon energy showed no yield in the range below 3.0 eV. As indicated in the figure there was severe activation at 3.9 eV and 4.1 eV, and as a result no readings were attempted above 4.1 eV. The yields obtained after this brief exposure to ultraviolet are shown by the dashed curve.

These data again indicate that if a quantitative correlation between the thermionic emission capability and the population of the donor levels is to be obtained a refined measuring procedure has to be developed. As indicated in the last report, it would be desirable to obtain a simultaneous measurement of the thermionic emission and the photoelectric yield under the normal operating condition of the cathode. The measuring equipment necessary for the simultaneous detection and separation of the thermionic and photoelectric emission has been developed and will be described in detail in the next section.

B. Experimental Apparatus for the Simultaneous Measurement of Thermionic and Photoelectric Emission.

The equipment used to simultaneously detect the photoelectric yield and thermionic emission from a coating has been developed in conjunction with the energy analyzer system. The equipment allows sufficient information to be obtained with the energy analyzer to permit a determination of the photoelectric emission energy distribution in terms of photoelectrons/quantum/eV and the thermionic energy distribution in terms of the fraction of the total emission at a given energy.

The basic principle used in the simultaneous detection is that of separating a dc thermionic current from an ac photoelectric current. The ac photoelectric current is produced by chopping the incident light beam used to measure the photoelectric yield. The ac and dc currents are separated by means of a transformer and the ac component is detected by a synchronous demodulator system. The synchronizing signal is obtained from a photoconductive cell exposed to the chopped light beam. The entire system will be described below for the sake of completeness and for future reference.

The schematic diagram of the monochromator and associated components is shown in Fig. 5. The light is resolved by the Bausch and Lomb 500 mm monochromater with a 600 groove/mm diffraction grating. This monochromator yields a linear dispersion of 33 Å/mm slit width; the resolution in terms of photon energy for 1.0 mm and 0.5 mm slit width is given in the table on Fig. 5.

Three light sources are available. The tungsten lamp and the H_2 arc have continuous spectra and are used in the total yield measurements, while the Hg-Ze arc has strong emission lines and is used for the energy analyzer measurements where a more intense, narrow width, light source is desirable. The light is focused into the monochromator by means of quartz lenses. The shutter and the filter used to eliminate the higher order wavelengths from the grating are located at the input of the monochromator. The light chopper wheel and the photoconductive cell used to drive the synchronous demodulator are located in front of the shutter. The output intensity of the monochromator is detected by deflecting about 10% of the beam, by means of a quartz plate placed at an angle in the beam, onto a phototube. Two phototubes are used to measure the light intensity in the range from 1.0 eV to 5.9 eV. The phototubes are calibrated using a vacuum thermopile as described in earlier reports. The output light from the monochromator is focused on the sample to be irradiated by means of quartz lenses.

The energy analyzer system is shown in Fig. 6. The electrons emitted from the cathode are accelerated by the cathode-grid potential, V_g, which is supplied by the batteries and can be selected by switch as shown. The electrons then receive an additional acceleration, or in some cases are decelerated, by the grid-analyzer supply, V_{ga}, connected between points G and B. The grid-analyzer potential is supplied by an Electronic Measurements dc power supply which provides a highly stable, well regulated, output voltage. The supply has been modified for use

as a dc-to-dc converter by using batteries to supply the input power. The reason for this is twofold; first, because of the large total voltage needed to operate the electron multiplier, the power supply must operate about 2 kV off ac ground, which would require the use of an isolation transformer. Second, the ripple from the power supply (250 μV), when operated on 60 cps, was sufficient to introduce a strong 60 cps component on the output current of the analyzer. The power supply voltage is controlled by an external 10 turn potentiometer which is driven by a reversible synchronous motor. The motor-potentiometer system has a revolution counter which activates the marker pen on the two channel time base recorder and hence, as the grid-analyzer potential is swept, the time axis of the recorder is calibrated by means of the marker pen. This marker system is necessary, as opposed to an x-y recorder, because of the large voltage, 2 kV, between the anode of the electron multiplier and the analyzer box. The use of an active power supply, instead of a simple battery-potentiometer type supply, is necessary because of the large dc thermionic currents which are drawn, which necessitate a supply with a low output impedance.

The electrons which enter the electric field-free region in the analyzer box are deflected by the magnetic field, directed perpendicular to the plane of the paper, and follow circular paths. The vertical magnetic field is supplied by a set of cube coils which enclose the entire tube structure. The dc coil current is supplied by a 12 V storage battery and is controlled by two parallel power transistors in series with the coils.

The tube is set up in the North-South direction and the earth's North-South magnetic field is cancelled by a second set of cube coils. The vertical coil current is determined by measuring the voltage drop across a 10 amp shunt by means of a Rubicon potentiometer. The magnetic field as a function of the coil current is calibrated by means of a Bell 120 gaussmeter.

Those electrons which have the proper entrance energy to enable them to traverse the analyzer box strike the first dynode of the Dumont 10-stage Ag-Mg multiplier structure. The multiplier voltages are supplied by means of the battery pack indicated. The shield around the multiplier is used to eliminate stray electrons from striking the multiplier and giving false readings of the emission current.

The anode-cathode switch, SW_2, is used to apply the electron multiplier anode current or the cathode current to the detection system. Switch SW_1, used to disconnect the accelerating potential, allows the determination of the dc thermionic emission. The filament power is obtained from a 12 V storage battery and the cathode temperature measured by means of the Pt - Pt + 10% Rh thermocouple.

The system used for the simultaneous detection and display of the ac photoelectric emission and the dc thermionic emission is shown in Fig. 7. The input dc plus ac current is applied to the input transformer and the 100 ohm or 10 KΩ sampling resistor. Since the dc current, under the condition desired during the measurements, is several orders of magnitude greater than the ac emission, the voltage across the sampling resistor will be a

measure of the dc current. This voltage is applied to the Keithley Model 199 milli-microvoltmeter which allows measurements of dc current from 10^{-9} to 10^{-3} amps.

The ac photoelectric current is applied to the input of the Tektronix Model 123 preamplifier through the transformer and the twin-T 60 cps reject filter. The amplified ac signal is then applied to the synchronous demodulator bridge circuit which is shown in detail in Fig. 8. The bridge is driven via the center-tapped transformer by the pulse generator circuit. The system is synchronized by means of the photoconductive cell mounted in the input chopped light beam of the monochromator system as shown in Fig. 5. The change in the resistance of the photo-conductive cell is detected by the two-stage, direct-coupled transistor circuit and the amplified signal is used to drive the first pulse generator. The gain control located in the base circuit of the input transistor is used to compensate for the different light intensities of the three light sources used.

The output pulse width of the first pulse generator is varied by means of the phase control. The trailing edge of this pulse is used to trigger the second pulse generator, which also contains a width control, duty cycle adjustment. This pulse, which can be moved in time with respect to the synchronizing wave form and whose duty cycle can be varied, is applied to the balanced bridge by means of the transformer. The bridge is thus opened and closed in synchronism with the incoming signal from the photoconductive cell. The inclusion of the phase and duty cycle adjustments allows the optimization of the demodulation

function. The trigger output and scope outputs are included for monitoring the demodulation process on an oscilloscope.

As shown in Fig. 7, the output of the demodulator is applied to the Keithley Model 603 electrometer which has a sensitivity range from 2.5 V to 1 V. The voltage detected by the electrometer is related to the equivalent dc photocurrent by measuring the dc photoelectric current and the ac photoelectric voltage output of the system at a given wavelength. This procedure eliminates the need for a recalibration of the monochromator light intensity system when using the chopped light.

The selector switch, SW_3, shown in Fig. 7, serves two functions. First, it determines the function of the Keithley 610 electrometer which is used to monitor the phototube current and also, in conjunction with the capacitors and resistors shown on section 5 of SW_3, is used as an operational amplifier to integrate the output of the 149 or 603. The second function of SW_3 is to select the proper amplifier output to plot on the two channel Texas Instruments time base recorder. The table indicates the function performed by the 610 and the data recorded. For example, in position 4, the photoelectric emission energy distribution is plotted on the A channel and the thermionic emission energy distribution is plotted on the B channel. The 610 integrates the photoelectric distribution and after the entire energy range has been covered the result of the integration is recorded on the A channel of the recorder by placing SW_3 in position 5. This switch, SW_3, makes it possible to obtain all the information necessary by following a sequence of operations for each pair of energy distribution curves taken.

Figures 9 and 10 show direct tracings taken from a typical run. The recorder traces from right to left in time, so the entire time interval presented runs from right to left on Fig. 9, then from right to left on Fig. 10. The numbered intervals at the center of the figures refer to the position of SW_3. In interval #1 the dc thermionic current from the cathode under test is obtained by removing the accelerating voltage and the effect on the thermionic emission of exposing the coating to light of the wavelength of interest is determined by opening and then closing the shutter. In 2 the photoelectric emission and the light intensity are determined. In 3 the output of the 603 amplifier is adjusted to near zero and the slope of the integrator (610) output recorded on channel A. In 4 the photoelectric and thermionic emission energy distributionsare recorded as a function of an increasing accelerating potential which is recorded by the marker system at the bottom of the figure.

During the entire run the analyzer geometry and magnetic field are held to transmit electrons of a fixed energy. Thus the outputs recorded at high values of V_{app} correspond to low-energy electrons leaving the cathode. In interval #5 channel A then records $\int I_{pd}$, which permits conversion of the distribution curve to photoelectrons per quantum per ev.

Intervals 6 through 8 are used primarily to permit a similar calibration of the thermionic distribution and, in addition, to verify both distributions.

In interval #6, shown on Fig. 10, the output of the 149 amplifier is adjusted to near zero and the slope of the intergrator output recorded on channel B. In 7 the distributions are again

determined, this time as a function of a decreasing accelerating potential, and in 8 the result of the integration is recorded on channel B. In 1 and 2 of Fig. 10 the data obtained previously in 1 and 2 of Fig. 9 are repeated as a check on the stability of the emission of the sample.

The entire procedure shown in Figs. 9 and 10 required about 3 minutes and in this time the following information was obtained: 1) the total thermionic emission from the cathode, 2) the total photoelectric yield from the cathode and the light intensity, which allows the determination of the total yield in photoelectrons/quantum at the given wavelength, 3) the effect of the incident light on the thermionic emission from the cathode, 4) the energy distribution of the thermionic emission and the integral of this distribution which, taken with the total thermionic emission from the cathode, allows the distribution plot to be converted to a plot of the fraction of the total emission in a given energy range vs. the electron energy (i.e., $\frac{N(E)dE}{N_T}$ vs. E), 5) the energy distribution of the photoelectric yield at the given wavelength and the integral of the distribution, which allows the distribution to be presented in terms of photoelectrons/quantum/eV as a function of electron energy, and 6) the stability of the sample is checked to determine the effect of the exposure to the incident light and the thermionic activation or deactivation resulting from the dc current drain.

This system has been used to obtain thermionic and photoelectric emission energy distribution data. These data will be discussed in the following sections.

C. Thermionic Emission Energy Distributions

Thermionic emission energy distributions have been used to evaluate the performance of the analyzer system. These distributions indicate that great care must be taken in the interpretation of the data obtained from the analyzer. Figure 11a shows a direct tracing of a thermionic emission energy distribution from a BaO coating, based on 0.024% MgNi, obtained with the cathode temperature at 700°C and with a magnetic field of 4.50 gauss. The vertical scale is the current measured at the final anode of the electron multiplier. The horizontal scale is the applied accelerating voltage applied between the cathode and the analyzer box. The grid voltage was set at 4.5 volts which was more than sufficient to eliminate space-charge effects. The electron energy increases from left to right.

Since the energy analyzer will accept electrons with energies within a small range, the observed output curve is not an exact reproduction of the energy distribution curve leaving the cathode. The form of the curve shown in Fig. 11a can be fit by assuming an energy distribution from the cathode of the form*

$$\frac{dI(E)}{I} = KEe^{-E/kT}dE \qquad (1)$$

This is the distribution of the emitted electrons with total energy between E and E + dE, as opposed to the distribution of those electrons with a normal directed energy between E_n and $E_n + dE_n$, which would be given by

$$\frac{dI(E_n)}{I} = K'e^{-E_n/kT}dE_n \qquad (2)$$

*I. L. Sparks and H. R. Philipp, J. Appl. Phys. 24, 453 (1963)

where K' is a constant which depends upon the system used to detect the electrons. In particular, if the analyzer accepts electrons with tangential components in the energy range from 0 to infinity, K' will equal 1/kT. As a range of the tangential component of E is reduced the value of K' goes to zero.

The distribution represented by (1) seems more reasonable to use in the present system since the tangential energies of the emitted electrons will be the order of kT and, for the acceleration voltages used, (the order of 6 volts) this will mean that the analyzer will accept all emitted electrons and hence the total energy distribution function should be applied.

The form of the energy distribution at the output of the analyzer can be obtained by integrating the energy distribution of the electrons leaving the cathode over the energy acceptance width of the analyzer. We let the analyzer have an acceptance curve idealized as a rectangle of width $2\Delta E$ centered about E. The integration must be carried out in two steps, the first being the region from $E = 0$ to $E = \Delta E$ and the second, the region from $E = \Delta E$ to infinity. This is necessary since both forms, (1) and (2), have value zero for $E < 0$. Thus, using form (1), one has as the output of the analyzer,

$$\frac{I(E)}{I} = \int_{\varepsilon = o}^{E + \Delta E} K' \varepsilon \, e^{-\varepsilon/kT} \, d\varepsilon \quad \text{for } -\Delta E \leq E \leq \Delta E, \qquad (1a)$$

and

$$\frac{I(E)}{I} = \int_{\varepsilon = E - \Delta E}^{E + \Delta E} K' \varepsilon \, e^{-\varepsilon/kT} \, d\varepsilon \quad \text{for } \Delta E \leq E < \infty. \qquad (1b)$$

These integrals yield

$$\frac{I(E)}{I} = K(kT)^2 \left[1-e^{-\frac{\Delta E}{kT}}\left(1+\frac{\Delta E+E}{kT}\right)e^{-E/kT}\right] \text{ for } -\Delta E \leq E \leq \Delta E \qquad (1c)$$

and

$$\frac{I(E)}{I} = K(kT)\, e^{-E/kT}\left[2E\sinh\frac{\Delta E}{kT} - 2\Delta E\cosh\frac{\Delta E}{kT} + 2kT\sinh\frac{\Delta E}{kT}\right] \qquad (1d)$$

$$\text{for } \Delta E \leq E < \infty$$

The equations (1c) and (1d) do have the form observed in Fig. 1a. The curve represented by (1c) has an inflection point at $E = kT - \Delta E$ and that by (1d) has an inflection point at $E = kT + \Delta E \coth\frac{\Delta E}{kT}$ and the combined curve has a maximum at $E = \Delta E \coth\frac{\Delta E}{kT}$.

In contrast to the above result, using the form for only the normal electrons, (2), we find on integration as before,

$$\frac{I(E_n)}{I} = K'\left[1 - e^{-E_n/kT}\, e^{-\Delta E_n/kT}\right] \text{for} -\Delta E_n \leq E_n \leq \Delta E_n, \qquad (2c)$$

and

$$\frac{I(E_n)}{I} = K'\left[e^{-E_n/kT}\sinh\frac{\Delta E_n}{kT}\right] \text{ for } \Delta E_n \leq E_n < \infty \qquad (2d)$$

These equations have no inflection points and do not resemble the observed curves. Therefore it appears that the form of the energy distribution of the emitted electrons which the analyzer will detect is that corresponding to form (1) and not (2).

Assuming that form (1) is correct, one can, to a fair approximation, determine from the thermionic plots, such as that shown in Fig. 1a, the value of ΔE and kT. This is done by assuming that $\coth \frac{\Delta E}{kT} = 1$ and by determining the point where $\frac{I(E)}{I}$ is a maximum, which will occur at $E = \Delta E$, the point where $\frac{I(E)}{I} = 0.264 \left.\frac{I(E)}{I}\right|_{max}$, which will be the first inflection point at $kT - \Delta E$, and the point where $\frac{I(E)}{I} = 0.736 \left.\frac{I(E)}{I}\right|_{max}$, which is the second inflection point at $\Delta E + kT$. These points are indicated in Fig. 1a along with the point $-\Delta E$ where the curve should rise above zero. Using the values for ΔE and kT determined from the analysis the shape of the energy distribution curve of the electrons leaving the cathode can be obtained and is shown in Fig. 11b. Note that, if $\Delta E/kT < 1$, the above approximations would still serve as the first step in an interaction solution for ΔE and kT.

The distribution plot shown in Fig. 11a is one of several obtained at the same temperature using different values of magnetic field. The relationship between the magnetic field in the analyzer and the energy of the electron, expressed in eV, which will be transmitted through the analyzer is given by

$$E = 0.0879\ B^2R^2$$

where E is in electron volts, B is in gauss and R is the radius of the transmitted electron trajectory in cm. This relationship should be useful in the determination of the zero of energy of the analyzer as is shown in Fig. 12. Here is plotted the applied accelerating voltage, V_p, at the peak of the thermionic

distribution as a function of the square of the magnetic field. From the slope of this line the radius of the transmitted electron trajectory is determined to be 1.36 cm compared to the design value of 1.5 cm. The curve, V_p vs. B^2, intersects the voltage axis at 3.0 eV, which corresponds to the contact potential difference between the coating and the Ti analyzer.

The value for the work function of Ti is about 3.9 eV which would yield a work function for the coating of 0.9 eV which is not reasonable. Other plots of V_p vs. B^2 have been obtained from this coating and in general these plots are not consistent as to slope and zero intercept. The slopes are all below 0.198, the value expected for 1.5 cm radius, and the zero intercept varies by as much as 1.0 eV. It is believed that this inconsistency is a consequence of a potential drop across the coating, which would be a function of the coating conductivity, and hence a function of temperature, and the current drain from the coating. This could be the source of the large variation in the zero intercept and also could effect the slope of the curve if the coating potential drop changed during a given set of measurements.

The values of ΔE and kT obtained from the curves used to determine the V_p vs. B^2 curve are also plotted in Fig. 12. The value of kT is fairly constant as would be expected since the temperature was not changed during the measurements. The value of ΔE increases with increasing magnetic field as would be expected because of the finite slit width of the analyzer. If we assume

$$V + \Delta V = 0.0879\ B^2\ (R \pm \Delta R)^2 \quad ,$$

then $\Delta V = 2(0.0879)B^2R\Delta R$ and, from the curve of ΔV vs. B^2, we obtain $0.023 = 2(0.0879)R\Delta R$. Using the value of $R = 1.35$ we obtain $\Delta R = 0.097$ mm. This value of ΔR is to be compared with the expected value of 0.25 which would be the theoretical value assuming the system were ideal. Any deviation from the optimum alignment of the three slits would tend to decrease this value, for example, if the vertical slit were not accurately located the ΔR would be reduced.

The curve labeled V_o in Fig. 12 was obtained by subtracting the value of ΔE from V_p at each point. As discussed above the distribution obtained peaks at ΔE instead of at $E = 0$, which is the value which should be plotted for an accurate determination of the zero of energy. This correction did not change the slope appreciably and lowered the contact potential difference to 2.8 eV. Thus this correction does not improve the situation with regard to an accurate determination of the zero of energy.

While obtaining thermionic emission distribution plots some additional structure was observed in addition to the major peak. These additional peaks are shown in Figs. 13a and 14a, which are direct tracings of the original recorder charts. Figure 13a was obtained with a magnetic field of 4.50 gauss, and is the superposition of two separate series made with a grid potential of 6 V and a grid-to-analyzer potential from 0 to 5 volts, #11, and with a grid potential of 9 volts and

a grid-box potential of -5 to 0 volts. The cathode temperature was 690°C and the total cathode current (temperature limited) was $I_T = 6.5 \times 10^{-5}$ amps. The major peak, at about 6.2 volts, was obtained with a detection sensitivity of 3×10^{-5} amps/cm, the smaller peaks, from 4.0 to 5.5 eV and from 6.7 eV to 11.0 eV, were obtained with a sensitivity of 3×10^{-7} amps/cm. A similar curve is shown in Fig. 14, with a different value of B and of V_g. The peaks observed are believed to result from an emission process from the coating as opposed to, for example, secondary emission from the grid, since the grid potential was changed from 3 to 9 volts in the curves shown in Figs. 13 and 14 and the extraneous peaks were always present.

One explanation of the extraneous peaks can be developed if the potential drop across the coating is taken into account. If a work function for Ti of 3.95 eV is assumed and if the slope obtained from the V_p vs. B^2 curve of Fig. 12 is used to derive the acceptance energy of the analyzer, E_a, the energy diagram of Fig. 13b is determined from the data shown in Fig. 13a. If it is assumed that the emitted electrons leave the coating with zero velocity, the position of the vacuum level of the coating with respect to the Fermi level of the base Ni can be determined by the following equation,

$$E_v = E_{fb} + (\phi_a + E_a) - (V_g + V_{ga}).$$

Therefore the strong peak at 6.2 volts applied would represent emission from the surface of the coating 1.08 eV above the Fermi level of the base Ni. The weak peaks at 4.3 and 4.7 volts applied would correspond to emission from the surface

2.58 and 2.98 eV above the base Ni Fermi level while the weak peak at 9.7 volts applied would correspond to the surface 2.42 eV below the base Ni Fermi level. The corresponding potential profile is shown in Fig. 13a. In this profile it has been assumed that the peaks at low applied voltage are a consequence of emission from the coating near the base and hence the value of 2.58 eV has been used for the work function of the coating. The strong peak at 6.2 volts applied is the emission from the coating near the surface of the coating and as indicated yields a contact potential difference between the emitting surface of 2.81 eV which agrees roughly with the value determined in Fig. 12. The weak peak at 9.7 volts applied then represents emission from the surface of the coating which reflects a large potential drop at the surface.

The thermionic emission energy plot shown in Fig. 14a was obtained in the same manner as that shown in Fig. 13a. In this case the magnetic field was 3.75 gauss which yields an acceptance energy for the analyzer, using the slope determined from Fig. 12, of 2.33 eV. The energy diagram of Fig. 14b is drawn under the same assumption used to construct Fig. 13b. The energy diagram derived from this distribution obtained using the lower magnetic field, and lower accelerating potential, has a lower potential drop at the surface of the coating and a slightly larger drop through the bulk. The work function of the coating, judged by the high energy distribution peaks, is about 2.6 eV in each case.

The value of the work function obtained from a Richardson plot on this cathode taken several days later, with the cathode in about the same state of thermionic activity, was 2.31 eV which is in fair argument with the value obtained from the energy diagrams of Figs. 13 and 14.

If the analysis of the thermionic emission energy distribution is correct the determination of the work function by means of determining the contact potential difference from a V_p vs. B^2 curve is in error. The position in energy of the major peak, which is the one used in the V_p vs. B^2 plots, will change depending on the potential drop across the bulk of the coating.

These data indicate that the interpretation of the photoelectric yield distribution curves, and thermionic emission distribution curves, will be difficult and that great care must be taken in the analysis of the curves. The data do, however, indicate that the use of the analyzer may yield further information regarding the potential profile of the coating while drawing current. Future experiments are anticipated in which distribution plots will be obtained as a function of the emission drawn from the coating, the acceleration potentials applied, and the temperature of the coating. These experiments should yield further information as to the cause of the potential profile, and as to the validity of the present interpretation of the distribution data on the basis of the potential profile indicated.

D. Photoelectric Emission Energy Distributions

Several photoelectric yield distribution plots have been obtained from this coating. These distributions have been obtained with the coating at near liquid nitrogen temperature up to 700°C. In the data obtained the position, with respect to the applied potential, of the photoelectric distribution plots appear to shift with temperature by an amount exceeding that which would be expected from the shift of the coating Fermi level. These shifts are not independent of the incident photon energy, that is, the shift at a given temperature is different for different photon energies. These anomalous shifts may be a consequence of the potential profile of the coating indicated above.

During the next interval further data will be obtained to examine more completely the coating potential profile. The information should allow a more detailed and dependable analysis of the photoelectric emission distribution plots and explain the large shifts observed in the position of the yield distribution curves as a function of temperature of the coating.

4. Thickness Studies

R. J. Soukup

A series of experiments aimed at determining the influence of the oxide coating thickness on cathode parameters was continued. A tube, SH5, was constructed using four standard cathode assemblies

located in side-arms. There was a change from previous tubes in this series in that Pt - Pt + 10% Rh thermocouples were used on these cathodes. The thermocouple junctions were located on the cathode sleeve 1/16" from the base nickel disk in all four cathodes. All cathodes employed 0.024% Mg-Ni alloy bases, and all were coated with $(BaSr)CO_3$ containing a radioactive tracer of Sr^{89}. The cathodes were shaved to thicknesses which ranged from 0.0014" to 0.0037", measured by comparing the radioactivity of the coating with that of a sample of known weight.

The structure was processed and the carbonate converted to the oxide following the procedure outlined in Scientific Report No. 2 of the previous contract.[1] The same change in procedure as discussed in Scientific Report No. 4 of this contract (elimination of the bakeout after conversion) was employed on this tube.

The tube was sealed off the processing pump and the filaments were turned on. After five hours of operation the sputter pump electrodes touched and welded together. During the attempt to shake the electrodes loose, one outer heat shield separated from its support. Operation was terminated on this cathode. The sputter pump electrodes were separated and pumping continued after a 1 hour interval, and life was re-initiated on the three remaining cathodes after 17 hours delay.

1. Scientific Report No. 2, Studies on Base Nickels for Oxide-Coated Cathodes, Contract No. AF(604)-389, P. 33

After 50 hours of continuous operation at a fixed cathode temperature of 800°C the pressure rose to the point where the tube was no longer suitable for measurements, the cathodes were all poisoned; a cracked press was discovered.

Examination of data taken after 28 hours of cathode operation, summarized in Table 1, indicate no clear-cut dependence of cathode properties on coating thickness. No detailed discussion will be presented since the measurements were taken after so short a life period.

Table 1

Comparison of emission, conductivity, and Sr evolution data from cathodes of varying coating thickness after 28 hours operation at 1073°K.

Cathode	Thickness	Pulse Emission, Amps/cm^2		Millimhos	Integrated Sr Evolution,
		J_D	J_{20}	cm^2	μgms/cm^2
SH5-FF1	0.0016"	3.9	7.3	50	3.5
SH5-FF4	0.0022"	2.2	5.3	10	0.5
SH5-FF2	0.0037"	3.4	7.2	47	0.75

III. Studies of Non-Thermionic Electron Sources

1. Introduction

Thermionic emitters are characterized in general as those in which the necessary energy required for electron escape at the surface is supplied thermally. The electron energy distribution in the emitter is in thermal equilibrium with the lattice, and only that portion of the electron population having surface-directed energies equal to or greater than the thermionic work function can escape. In addition to thermal excitation, it is possible to supply excess kinetic energy to electrons in a solid so that these "hot electrons" can escape.

To show promise of providing a useful electron source, any non-thermionic emitter should satisfy a number of criteria. These include the following:

a) The current density, and total current per device, must be adequate.

b) The excitation energy should not be too difficult to supply, in comparison with thermionic excitation.

c) The velocity distribution of the emitted electrons must be limited to facilitate focusing, modulation, and other utilization requirements.

d) Random fluctuations, or noise, must be limited.

e) Lifetime of the source, in its projected application and environment, must be adequate.

The above list is not exhaustive, and the relative importance of each criterion will of course depend upon the projected application.

In the studies being undertaken by this project, two general means of exciting the electrons are being considered. In both, the excitation energy will be in the form of externally applied electric fields (as in normal field emission). One scheme involves the acceleration of electrons while passing through a thin film insulator and the second involves the co-operative acceleration of electrons in a superconductor.

The first of these two emission mechanisms requires electron tunneling through a thin insulating film and subsequent penetration of a thin metal overlayer into vacuum.* Devices to observe these phenomena consist of a metal base, a thin insulating film (of the order of 100 Å), and a thin metal overlayer. When a potential of a few volts is applied between the metal layers an electric field of the order of 10^7 volts/cm is established in the insulating film. Fields of this magnitude are large enough to cause field emission of electrons from the negative metal through the potential barrier of the insulator into the positive metal film. If now this metal film is thin enough an appreciable fraction of the electrons may be able to reach the metal vacuum interface with energy greater than the work function and pass into the vacuum. This last requirement implies that the thickness of the insulator be chosen such that a voltage greater than the metal-vacuum work function can be applied before sample damage or breakdown occurs.

*C. A. Mead, Proc. IRE 48, 359, March (1960).

The possibility of obtaining enhanced emission from a superconducting field emitter has also been established. It is argued that, if a superconductor is made to operate under conditions approaching those which would return it to the normal state, the density of coupled electrons carrying current in the bulk of the material will approach zero. As a consequence, the surface-directed kinetic energy of these electrons will permit their escape over the barrier without tunneling. Experimental results have been presented for Nb and Ta emitters which show that the I-V characteristic of a superconducting field emission diode passes through a negative-resistance region as the emitting tip makes a transition to the normal state. The existence of such a negative-resistance region is predicted by the model in which the emission enhancement occurs as a consequence of "hot" electrons passing over the potential barrier rather than tunneling through it. Further experiments aimed at utilizing these hot electron effects in superconductors have been undertaken, but their discussion will be deferred until techniques and results have been established.

As an additional possibility, the extraction of electrons from a high-vacuum liquid-pool arc has been suggested as providing a potentially useful electron source. Experiments aimed at establishing a high-vacuum arc from a low vapor pressure (gallium) pool cathode are therefore also described in the following sections.

2. Thin-Film Dielectric Studies

A. $Al-Al_2O_3-M$ Diode Properties — O. L. Nelson

An understanding of the operation of thin film tunnel current devices requires a knowledge of the effect on the I-V characteristics of the insulating film formation methods. Three methods of oxide formation of Al underlayers have been tried; anodization, heating in an O_2 atmosphere, and bombardment by oxygen ions from a plasma. The first method produces oxide films which are continuous, quite reproducible and can be formed to predetermined thicknesses. The second method has been tried several times at different temperatures for varying times but has not resulted in the formation of films with good insulating properties. These results were presented in Report No. 5 of this series.

A tube structure was described which was used for oxygen ion bombardment of the metal underlayers, and a diagram of this structure was shown in Fig. 19 of Scientific Report No. 5. Results were presented from several attempts to form insulating films, all of which were not successful. A further trial of this method has been performed.

The underlayers of four samples, Al-51, 52, 53, 54, were deposited simultaneously, each 1" in length and 0.02" wide, each on a fire-polished glass substrate. Two of these, Al-51 and 52, were anodized in ammonium tartrate at 5.0 V for three minutes. Al-53 and 54 were not anodized. Then Al-51 and 54 were mounted in the plasma tube. This structure consists of a W ribbon electron source and an anode to sustain the plasma discharge. The electrons are constrained by an axial magnetic

field to a beam of approximately 1/4" in diameter. The plasma was established at an oxygen pressure of 3×10^{-3} Torr with 30 V anode potential and 5 mA total current. The samples, Al-51 and 54 and a W mesh between them and the plasma, were biased 4 V ac rms with respect to the anode (plasma) potential for 45 minutes. The total ac current to screen, samples and holders was about 20 μA.

Each of the four samples were then inserted in an evaporator tube and had nine 0.05" wide overlayers vacuum-deposited across the underlayer; 4 were Au, 5 were Al. Note that no attempt was made to form an oxide layer on Al-53, except that it was stored at atmospheric conditions in a dust-tight container (in an air-conditioned area) for about 3 weeks. I-V characteristics were obtained from the samples, and the results of initial measurements with positive overlayer bias are shown in Table I.

Table I

Voltage required to pass 0.1 μA through the active areas, positive overlayer polarity

	Overlayer				Al	Au			
Sample	1	2	3	4	5	6	7	8	9
Al-51	0	2.6*	2.7	3.0*	3.0	2.9	2.0	2.0	0
Al-52	2.2	2.2*	2.0*	2.2*	0	0	0	3.3	2.7
Al-53	0.004	0.004	0.003	0.003	0.003	0.04	0	0	0.02
Al-54	0	0.01	0.02	0	0	0.15	0.23	0.25	0

*sample broke down during measurement, becoming a short.

From the table two inferences can be drawn. First, the oxygen bombardment did not destroy the previously formed anodized film. Neither anodized sample (Al-51 and 52) yielded consistent results, and both were subject to breakdown, but it appears that Al-51 was not deteriorated by the bombardment.

Secondly, sample Al-54, which was bombarded, requires substantially higher voltages to pass 0.1 μA than does Al-53, stored in air. Further, all characteristics from Al-53 were resistive up to 0.1 μA current, and all except #6 and #9 were resistive up to 5 μA. The maximum resistance was 4×10^5 ohms from #6. The I-V characteristics from Al-54, however, showed continuous curvature from the origin, and areas #7 and #8 showed resistances at the origin in excess of 5×10^6 ohms.

It appears from the results obtained from these four samples that biasing a metal film so as to attract oxygen ions to it from a plasma can form an insulating oxide film. More work would be necessary to refine the technique, however. It is felt that, for the present, the anodized films show more promise.

To investigate the effects on the insulating properties of anodized Al_2O_3 films caused by different anodizing and processing techniques, a series of samples have been constructed. Al underlayers 1" x 0.1" were deposited on fire-polished glass substrates of four samples simultaneously, after baking the system at 400°C. The anodizing solution and also the heat treatment after anodization were varied, but the maximum anodization voltage and current were held constant. The voltage was increased holding the current constant at 60 $\mu A/cm^2$

until a voltage of 6 V was reached, and then held at this value until the current decreased below 5 $\mu A/cm^2$ or for 6 minutes, which ever was longer. The samples which received the various processings are shown in Table II. Five 0.05" wide Al overlayers and four Au overlayers were vacuum deposited.

Table II

Anodization and Processing Schedule

Heat treatment after anodizing, before overlayer deposition	3% tartaric acid and NH_4OH to pH 5.5	3% tartaric unadjusted	3% citric acid and NH_4OH to pH 5.5	3% citric unadjusted
Unbaked	Al-43	Al-58	Al-41	Al-55
Baked 1 hr. at 110°C in air	Al-44	Al-42	Al-57	Al-56
Baked 1 hr. in air and 1 hr. in vacuum at 110°C	Al-48	Al-47	Al-61	Al-60
Baked 1 hr. at 110°C in vacuum	Al-49	Al-59	Al-62	Al-50

Preliminary measurements were made of the I-V characteristics for each active area up to about 2μA total current, with the overlayers biased positively. The results are shown in Table III, where the voltages necessary to pass 1μA are tabulated for each overlayer. The samples are arranged in construction groups. (The deposition of underlayers and overlayers were performed simultaneously on each group of four.) It can be seen from Table III that the voltage values vary by almost as much as a factor of two for different samples, but for a particular sample, the agreement among Al or Au overlayers is quite good.

For further comparisons, overlayers #4 were chosen except for those cases for which it was atypical and #3 overlayer was used. These I-V plots are shown in Fig. 15. Note that the current scale is 1 μA/in except for Al-48, #4, with 0.1 μA/in. This sample showed breakdown at higher current levels. Also for Al-61, #3 and Al-62, #4, each have a corrected and uncorrected characteristic. The deviation of the uncorrected curves is believed to be a consequence of the measurement equipment or the leads with silver paint contacts. (The resistance of the paint is quite high immediately after application, decreasing to a low value in about a day.) Subsequent measurement on the following day yielded characteristics similar to the corrected ones shown in the figure. As can be seen, the voltage values necessary for appreciable current flow cover quite a large range. In addition to this, the shape of the curves (in particular the amount of hysteresis) varies from one sample to another. The hysteresis is not completely determined by the sample, since the speed at which the characteristic is traced out can affect the magnitude of the shift to higher voltages, as can the maximum current value. The shape of the voltage-increasing portion of the curve is probably more dependent on the measuring speed and maximum current than the voltage-decreasing portion, and for this reason the voltage-decreasing portion of the characteristics will be used for further analysis.

Fowler-Nordheim plots of log I/V^2 vs. $1/V$ were obtained for the voltage-decreasing portion of the characteristics discussed above, and are shown in Fig. 16. The curves for Al-61

Table III

Voltages Required to pass 1 μA, with Overlayer Positive

Sample No.	Overlayer No. 1	2	3	4	5	6	7	8	9
Al-41	0	1.1**	3.55	3.6	0	4.3	4.2	4.3	0
-42	---	3.8	3.8	3.85	0	0	4.10	4.0	4.05
-43	3.75*	0	--*	0	--*	3.95	4.0	0	0
-44	--*	0	3.6	3.5	--*	0	4.4	4.4	4.4
Al-47	---	---	3.1	3.2	3.25	3.95	3.9	3.85	3.9
-48	--*	--*	---	---	---	---	---	---	---
-49	2.95	0	3.1	3.35	0	4.1	0	0	0
-50	2.95	3.05	3.05	3.25	3.3	4.05	3.95	3.9	3.95
Al-55	2.95*	0	3.05	3.05	3.1	3.75	0	3.65	3.7
-56	0	3.25	3.2	0	3.3	3.8	3.85	3.2**	3.85
-57	0.6+	3.15	3.1	3.1*	3.15	3.8	3.8	3.8	0
-58	0.7+	3.4	3.35	3.45	3.25	3.85**	1.0**	0	3.1**
Al-59	1.3**	0	2.7	2.7	2.7	0	3.8	3.85	1.0**
-60	--*	2.7	2.7	2.7	2.7	3.8	3.8	3.8	0
-61	2.65	2.5	2.55	2.55	0	0	3.4	3.55	0
-62	2.55	0	2.1*	2.4	2.4	0	0	2.7**	0.2+

\+ - showed resistive behavior at the origin, less than 1/2 megohm.

* - active area became shorted during measurement.

** - characteristic was erratic, with sudden changes in current.

and 62 were obtained from the corrected I-V characteristics. The Fowler-Nordheim tunnel current equation can be written in the form $I/I_o = (V/V_o)^2 e^{-V_o/V}$, where I_o and V_o are parameters of the sample. Using the free electron mass, $V_o = 6.8 \times 10^7 \phi^{3/2} d$, volts, where d is the oxide thickness in cm, and ϕ is the effective potential barrier at the metal-oxide interface measured in eV. The oxide thickness of anodized Al is about 12-13 Å per volt anodizing potential. The anodizing potential for all of these samples was 6 V, so the oxide thickness is about 75 Å. Small variations in the thickness of the several samples are possible, however, because the maximum voltage was maintained longer on some samples, as previously mentioned.

Values of V_o were obtained from the curves of Fig. 16. The curves are not all straight lines, but are linear enough to obtain slopes. These values of V_o are shown in Table IV, as well as values of V_o obtained from the voltage-increasing portions of the characteristics, the voltage values for 1 μA current for both increasing and decreasing portions, the voltage shift at 1 μA from increasing to decreasing portions, and the ratio of the V_o values. A careful examination of these parameters indicates no clear correlation between oxide preparation and I-V characteristics. There are some trends, which may or may not be causal; e.g., the unbaked samples appear to have the largest values of ΔV_o. The most definite correlation, however, appears to be the similarity between samples prepared as a group; for example, samples Al-59, 60, 61, 62, all prepared simultaneously, show V(1 μA) values considerably lower than the others.

Table IV

Sample	Over-Layer	Heat treatment	Anodizing Solution	Voltage Increasing		Voltage Decreasing			
				V_o	V(1μA)	V_o	V(1uA)	ΔV (1μA)	$\frac{V_o \text{decr.}}{V_o \text{incr.}}$
58	4	none	tartaric	38	3.5	77	3.65	0.2	2.0
41	4	"	citric pH 5.5	36	3.6	72	3.8	0.2	2.0
55	4	"	citric	44	3.05	71	3.2	0.15	1.6
44	4	air	tartaric pH 5.5	40	3.5	76	3.65	0.15	1.9
42	4	"	tartaric	46	3.85	57	3.95	0.1	1.2
57	3	"	citric pH 5.5	49	3.1	74	3.25	0.15	1.5
56	3	"	citric	53	3.2	71	3.3	0.1	1.3
48	4	air, vac	tartaric pH 5.5	38	---	66	---	---	1.7
47	4	"	tartaric	47	3.2	72	3.3	0.1	1.5
61	3	"	citric pH 5.5	27	2.55	52	2.8	0.25	1.9
60	4	"	citric	38	2.7	61	2.75	0.05	1.6
49	4	vac	tartaric pH 5.5	49	3.35	60	3.4	0.05	1.2
59	4	"	tartaric	37	2.7	50	2.8	0.1	1.4
62	4	"	citric pH 5.5	25	2.4	52	2.55	0.15	2.1
50	4	"	citric	61	2.25	75	3.3	0.05	1.2

The results presented for this series of samples are preliminary, but indicate that the electrical properties of the oxide are quite insensitive to the method of oxide preparation, at least to those methods used here. Further measurements will be made on these samples, in particular measurements at 77°K, and negative overlayer bias measurements. Some correlation between electrical properties and oxide preparation may be found from these measurements.

B. Electron Emission From Thin Film Diodes E. D. Savoye

Studies of electron emission into vacuum from thin-film "sandwich" devices have been continued during the present interval. Preliminary attempts to observe such emission from $Ta-Ta_2O_5-M$ tunneling samples were discussed in Scientific Report No. 4 of this series. These studies were unsuccessful; no emission into vacuum was observed from these devices.

In order to permit development of the experimental procedures requisite to such investigations, and to provide a basis for more extended studies of the Ta and other similar systems, it was decided to examine electron emission processes from well-established systems.

Kantor and Feibelman* have studied electron emission processes from $Al-Al_2O_3-Au$ sandwich devices, and the experimental procedures which they described were adapted for our use.

A simplified vacuum tube structure has been designed for these experiments. The structure is designed for immersion into liquid N_2, to allow low-temperature measurements; and provision is made for the overlayer deposition to be performed in situ.

*H. Kantor and W.A. Feibelman, Westinghouse Research Paper 62-112-252-P2.

The sample configuration is that of crossed metallic strips, separated by a thin oxide layer. An Al strip, 0.020" width and of about 5000 Å thickness, vacuum-deposited upon freshly fire-polished glass, was anodized to the desired oxide thickness in ammonium citrate.* Three pairs of Au tabs were then vacuum-deposited adjacent to but not overlapping the Al strip, and electrical connections were made to the Au tabs and to the Al underlayer strip with silver paint. Au overlayer strips were deposited in the final tube structure, connecting each pair of Au tabs. A measurement of the resistance of each overlayer strip could therefore be made, and hence the thickness of the Au film could be determined.

After mounting the anodized Al sample with Au tabs in the vacuum tube, the structure was evacuated, using a Ti sputter pump,** and baked for one hour at 100°C. The Au filaments were then outgassed; the tube was sealed off from the pump station, and the small Ti sputter pump associated with the structure was put into operation. The pressure in the tube during subsequent processing was of the order of 10^{-11} Torr, except during Au deposition, when the pressure rose to nearly 1×10^{-7} Torr.

* The electrolyte was a solution of 3% citric acid, adjusted to pH 5.5 with NH_4OH. The samples were anodized at a current density of 400 $\mu A/cm^2$ to the desired voltage, and then held at constant voltage for at least 9 minutes after which they were baked in air at 150°C for one hour.

**The details of the pump-down procedure were presented in Scientific Report No. 4, of this series, Sec. III-2C.

Measurements were taken according to the following procedure. A thin layer of Au was deposited from the filament onto the sample, through a mask arranged so that three overlayer strips were formed upon the sample simultaneously; each connecting one pair of Au tabs. The deposition was performed with the tube at room temperature; and the resistance between the center pair of Au tabs was monitored during the deposition. Immediately following the Au deposition, the resistance of each overlayer was measured. The sample was then connected according to the four-terminal measurement circuit, shown in Fig. 17, and emission measurements were made. The tunneling current, I_t, was plotted vs. the tunneling voltage, V_t, on an X-Y recorder, and the emission current, I_e, was plotted vs. V_t simultaneously on a second X-Y recorder. Alternatively, I_t, at a fixed tunneling voltage, was monitored on one recorder while I_e was plotted versus a retarding potential, V_R, on the second recorder. Measurements were made both at room temperature and at liquid N_2 temperature. After completion of the measurements, additional Au could be deposited upon the sample, and the emission measurements repeated for thicker Au overlayers. Results could thus be obtained for a given sample over a range of overlayer thicknesses, thereby facilitating studies of the dependence of the results upon overlayer thickness.

Results have been obtained thus far for two samples; Al_c - 3 and Al_c - 6, anodized to oxide thicknesses of 78 Å and 104 Å respectively. Because of the preliminary nature of these experiments, and because of the limited data available, no attempt at

detailed analysis will be made. A description of the general results obtained will, however, be given.

The $I_t - V_t$ characteristics of the samples when first measured gave reasonable fits to Fowler-Nordheim plots at room temperature and at liquid N_2 temperature. It was observed that I_e vs. V_t would also fit a Fowler-Nordheim plot, but with a slope different from that of the $I_t - V_t$ plots.

The $I_t - V_t$ characteristics showed aging and hystersis effects similar to those noted earlier for $Al-Al_2O_3$ samples anodized in tartaric acid. After operation at high current levels, the samples were subject to breakdown. The breakdown usually occurred as a transition to a new I-V characteristic rather than to a short circuit. The main feature of the new I-V characteristic was an increased conductivity at low voltages, and it was found that most and, is some cases, all of the increase could be eliminated by applying an even larger bias voltage to the sample. The current would then suddenly decrease, and the increased conductivity was removed, as a transition occurred to an I-V characteristic similar to the original $I_t - V_t$ characteristic. It was noted that, in the presence of the increased conductivity, the $I_t - V_t$ characteristic did not fit the Fowler-Nordheim relationship; however, a plot of I_e vs. V_t was in general unchanged in the presence of the increased conductivity. These results indicate that the increased conductivity was a result of mechanisms other than electron tunneling from the Al underlayer, acting in superposition with the retained tunnel current.

The current transfer ratio, α, can be defined as $\alpha = I_e/I_t$; the ratio of the emitted current to the sample current at fixed voltage. The results obtained for this ratio from sample Al_c-3 for various overlayer thicknesses are shown as semi-log plots in Fig. 18. The data presented were obtained with the sample held at liquid N_2 temperature, in order to minimize aging and hystersis effects.

Two main features of these curves are of interest: (a) the curves for different overlayer thicknesses have roughly the same shape, but the level decreases as the overlayer thickness is increased. A decrease in α with increasing overlayer thickness would be expected in the case where the injected electrons must pass through the Au overlayer itself, rather than through small holes in the Au film. (b) The transfer ratio α increases as the sample voltage increases. On the basis of a model in which the injected electrons interact primarily with the conduction electrons in the Au overlayer film, one would expect the transfer ratio to decrease with increasing injection energy, for mono-energetic injection.* The experimental result; that α increases with increasing energy, can be understood in terms of a spread in energy of the injected electrons such that at the higher voltages, a greater fraction of the injected electrons have sufficient energy to escape. These considerations do not rule out the possibility of the presence of pinholes in the Au film, however, since a similar discussion can be given in terms of escape of electrons through such small holes.

* H. Thomas, Z. Physik 147, 395 (1958).
J. J. Quinn, Phys. Rev. 126, 4, 1453 (1962).

In the present measurement, the partial breakdown of some samples, and subsequent "healing" which was described, render precise interpretation of the results difficult. In particular, doubt is cast upon the interpretation of the quantity α in those cases where the $I_t - V_t$ characteristics do not fit the Fowler-Nordheim relationship. During the next interval these measurements will be continued, and efforts will be made to produce samples less susceptible to breakdown, in order that more meaningful results can be obtained. In addition the possibility of obtaining measurements on a pulse, rather than a dc basis, in order to minimize sample breakdown, aging and hysteresis effects, will be explored.

3. Arc Discharges from a Ga Pool Cathode

R. A. Pedersen

As a consequence of the high current and low voltage-drop properties of arc discharges, it was thought that it might be possible to use an arc as a primary electron source with a comparatively high efficiency and of very high current capabilities. In an arc discharge the voltage drop is usually very near the ionization potential of the cathode material and therefore, if the electrons could be extracted for use as free electrons, the energy required to extract an electron would be of the order of this ionization potential.

The original plan was to draw an arc discharge from a gallium pool to a main anode and then try to draw a fraction of the electrons to an auxiliary anode. Gallium was chosen as the

cathode material because of its low vapor pressure, making it suitable for use in a high vacuum system, and its low melting point, being a liquid at room temperature.

A structure (Fig. 19) was built to (1) determine if an arc could be drawn from the gallium pool and (2) if such an arc could be started, to see if electrons could be drawn from the discharge region to the auxiliary anode. The method used to attempt to initiate the arc was (1) raise the level of the gallium pool by lowering the displacement weight with a magnet, (2) pass dc current through the pool-anode junction, and (3) lower the pool level to break the contact. The arc was then supposed to start at the point where the contact was broken. The structure was submerged in a water bath throughout the experiment to provide cooling. A similar structure was used with Hg rather than Ga; it was found that the mercury pool discharge could be started and controlled readily.

The power was supplied by a 110-220 volt dc motor-generator set with a current rating in excess of 100 amps. During the trials the current was limited to 50 amps, which was considered to be the maximum current which could be carried safely by the structure. No continuous arc discharge was observed at any time. At 50 amps a short bright flash with subsequent flashing of gallium throughout the tube was observed. This was believed to be an instantaneous arc which occurred at the time that the junction was breaking but it was not possible to sustain the arc.

It was also attempted to start the arc by placing a high voltage rf power supply in series with the dc line but this was also to no avail. The rf power was supplied by a 30 kV, 2

megacycle starter designed for starting a mercury-xenon arc lamp. In this case dc currents of 15 amperes were still cleanly interrupted by separating pool and anode.

The failure to initiate an arc at the current levels that were used led us to termination of this study, believing that the power levels that would be involved, if the arc could be initiated at all, would not be practical.

It should be pointed out that the use of a Ga pool as a high-current, high-voltage switch would appear quite practical, with ratings far in excess of mercury pool switches. Currents of 50 amps from a line supply of 220 V dc were interrupted repeatedly. In several cases the primaries of three 220 volt, 1.75 KVA transformers were connected to add inductance in series with the tube, in an attempt to sustain the current during separation of the ω anode from the Ga pool. In these attempts the currents of up to 20 amperes were still cleanly interrupted until arc breakdown in the input leads to the transformers occurred at an estimated several kilovolts.

It should be recalled that the tube was not designed for optimum use as a switch; the sharp W electrode and deliberately minimized separation distance would both tend to enhance any possible breakdown.

IV. Conclusions

It has been demonstrated that a controllable vapor pressure of the alkaline-earth metals can be established above an oxide cathode and that this heated anode structure will be suitable for further measurements.

The time dependence of the photoelectric yield from an oxide cathode following a life period at 800°C is not a consequence of a donor diffusion process as reported previously, but rather is a consequence of a donor destruction process caused by the coating environment. The system constructed for the simultaneous detection of the thermionic and photoelectric energy distribution has been evaluated, and the results indicate that the system will be adequate. The potential profile of a BaO coating while drawing dc cument has been derived using the energy distribution of the thermionic emission. The potential drop is composed of two regions, the first being a drop in the bulk and the second a sharp drop at the surface of the coating.

Oxide films on Al thin film tunnel current samples formed by bombardment of the Al by oxygen ions were found to be poor insulators. Al_2O_3 films formed by anodization of Al in 3% citric, 3% tartaric, both unadjusted and adjusted to pH 5.5 with NH_4OH, and with different heat treatments were fabricated. The preliminary results indicate that the insulating properties of the films are quite insensitive to the electrolyte used or the subsequent heat treatments. All samples yielded qualitatively similar I-V characteristics.

Experiments with Al-Al_2O_3-Au thin-film sandwich devices were described in which emission into vacuum was observed. Preliminary results were obtained for the current transfer ratio, α, as a function of the Au overlayer thickness, for Au thicknesses in the range 100Å to 176 Å. These preliminary results indicate that the current transfer ratio decreases with increasing Au film thickness, at a given sample voltage; and that the ratio increases with increasing sample voltage for a given Au overlayer thickness. Transfer ratios in the range 10^{-5} to 10^{-3} were observed in these experiments.

It has been found that a sustained arc cannot be drawn from a Ga pool cathode to a withdrawing W electrode even with currents of 50 amperes and applied voltages in the kilovolt range.

V. Personnel Employed on Contract

	Percent	Man Months
W. G. Shepherd	100.	1
D. E. Anderson	66.7	3
[1]D. A. Campbell	100.	3
O. L. Nelson	54.	3
E. D. Savoye	75.	3
R. H. Springer	100.	3
C. A. Stolte	100.	3
[2]D. E. Garfin	75.	2.5
[3]Douglas Lood	88.	2.5
[2]R. A. Pederson	75.	2.5
R. J. Soukup	90.	3
[2]T. J. Szczech	100.	2.5
Secretary	50.	3
Engineer	15.	3
Laboratory Technical Assistants		3,136.5 Man Hours

[1]Terminated on 8/31/62.

[2]Appointed Research Assistants on the contract beginning 6/16/62.

[3]Terminated on 8/15/62.

STRUCTURE USED IN CONTROLLED ALKALINE EARTH VAPOR STUDIES

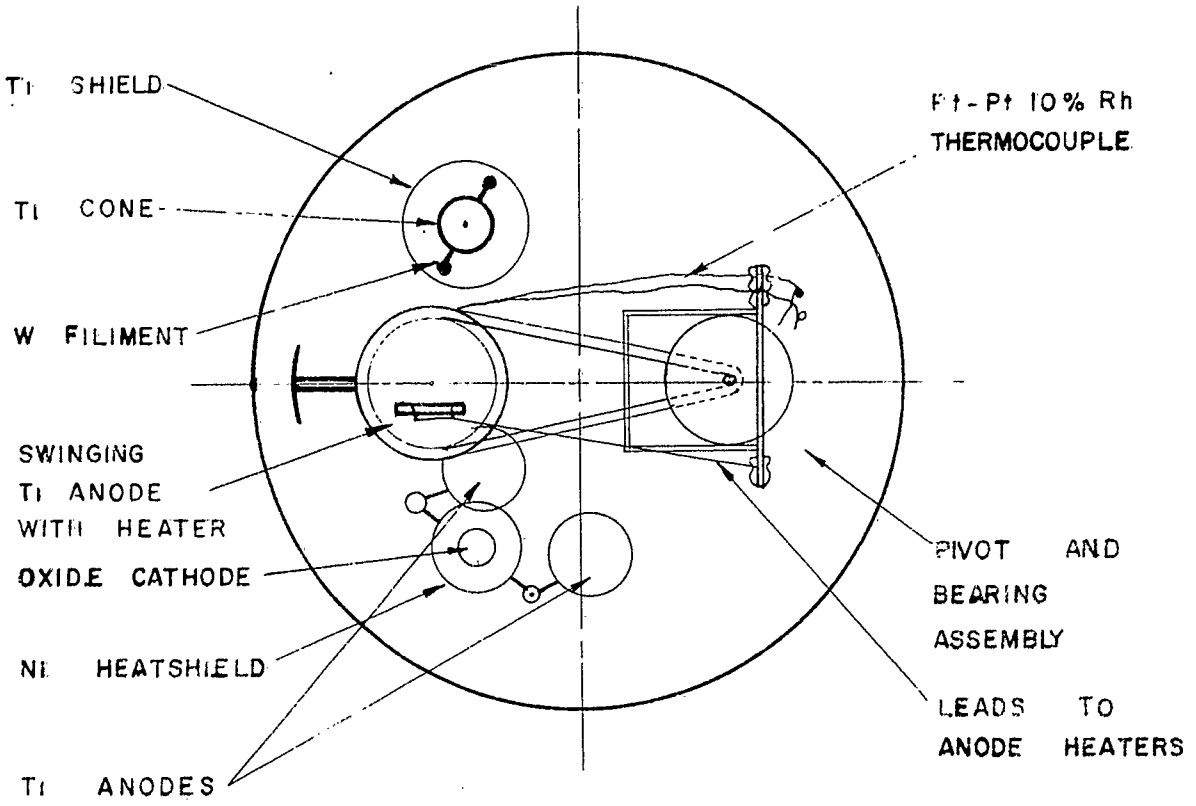

FIG. 1

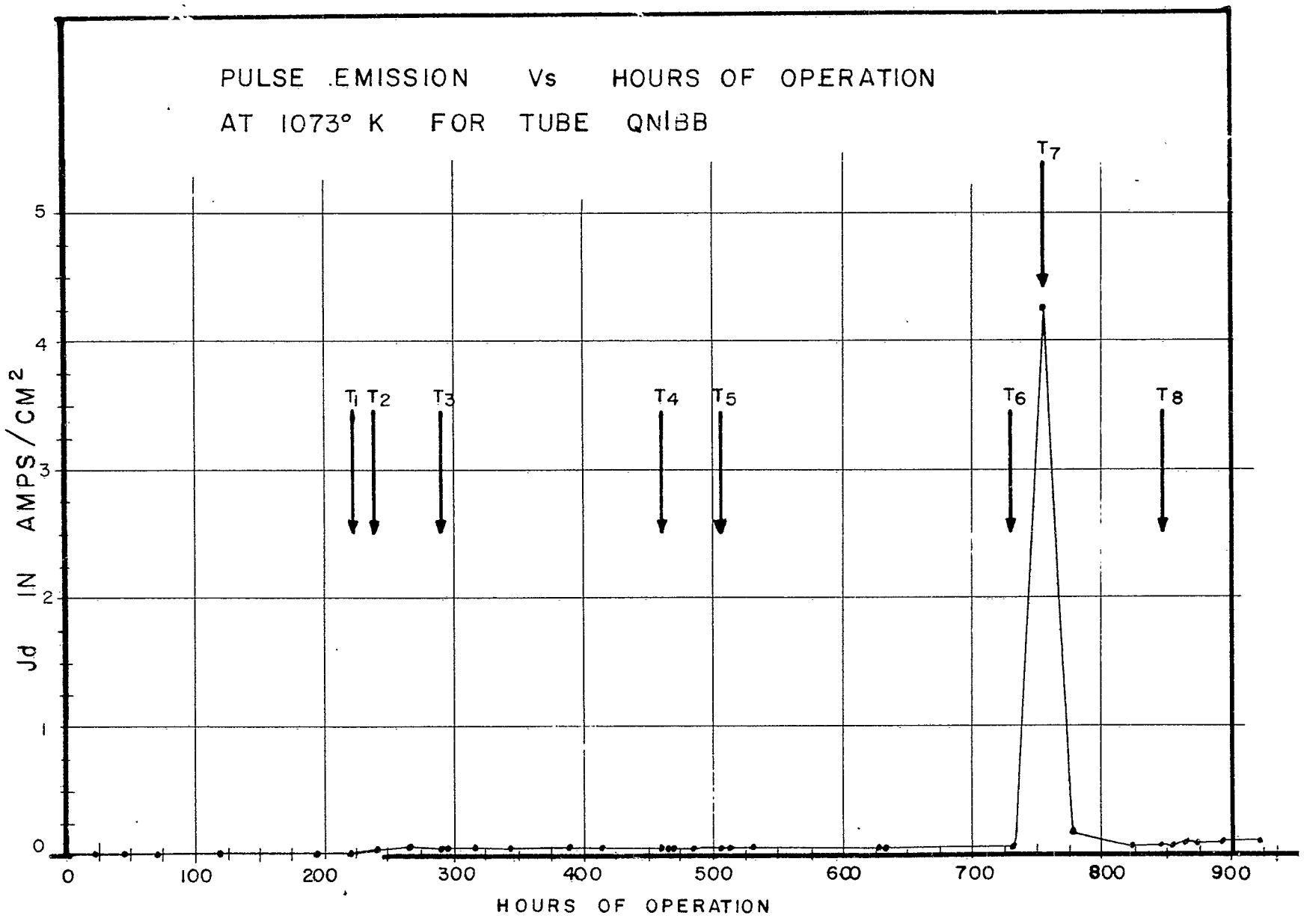
PULSE EMISSION Vs HOURS OF OPERATION
AT 1073° K FOR TUBE QN1BB
Jd IN AMPS/CM²
HOURS OF OPERATION
T1 T2 T3 T4 T5 T6 T7 T8
0
1
2
3
4
5
0 100 200 300 400 500 600 700 800 900

FIG. 2

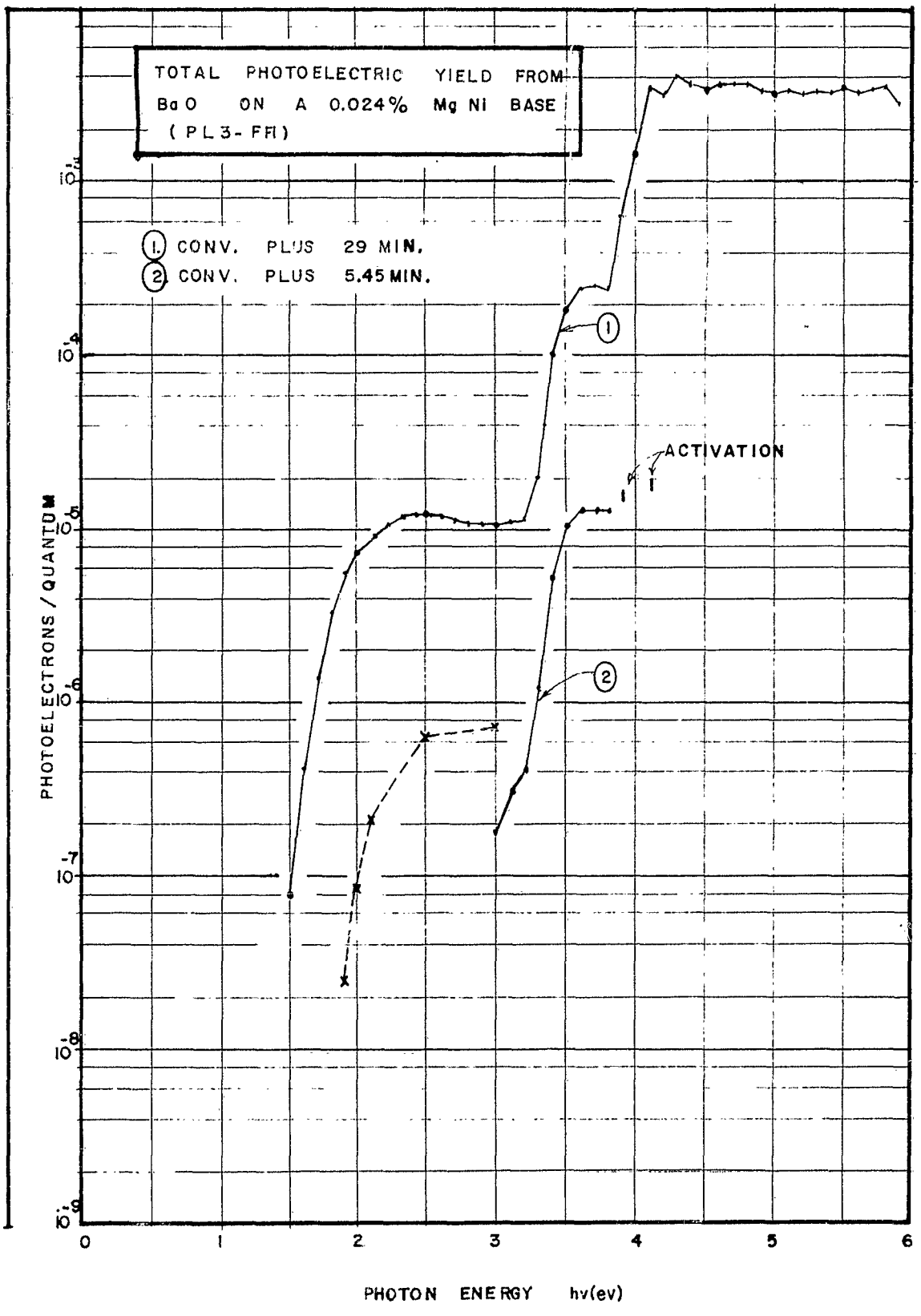
TOTAL PHOTOELECTRIC YIELD FROM
Ba O ON A 0.024% Mg Ni BASE
(PL 3- FFI)
1. CONV. PLUS 29 MIN.
2. CONV. PLUS 5.45 MIN.
ACTIVATION
PHOTOELECTRONS / QUANTUM
PHOTON ENERGY hv(ev)
0
1
2
3
4
5
6

FIG.3

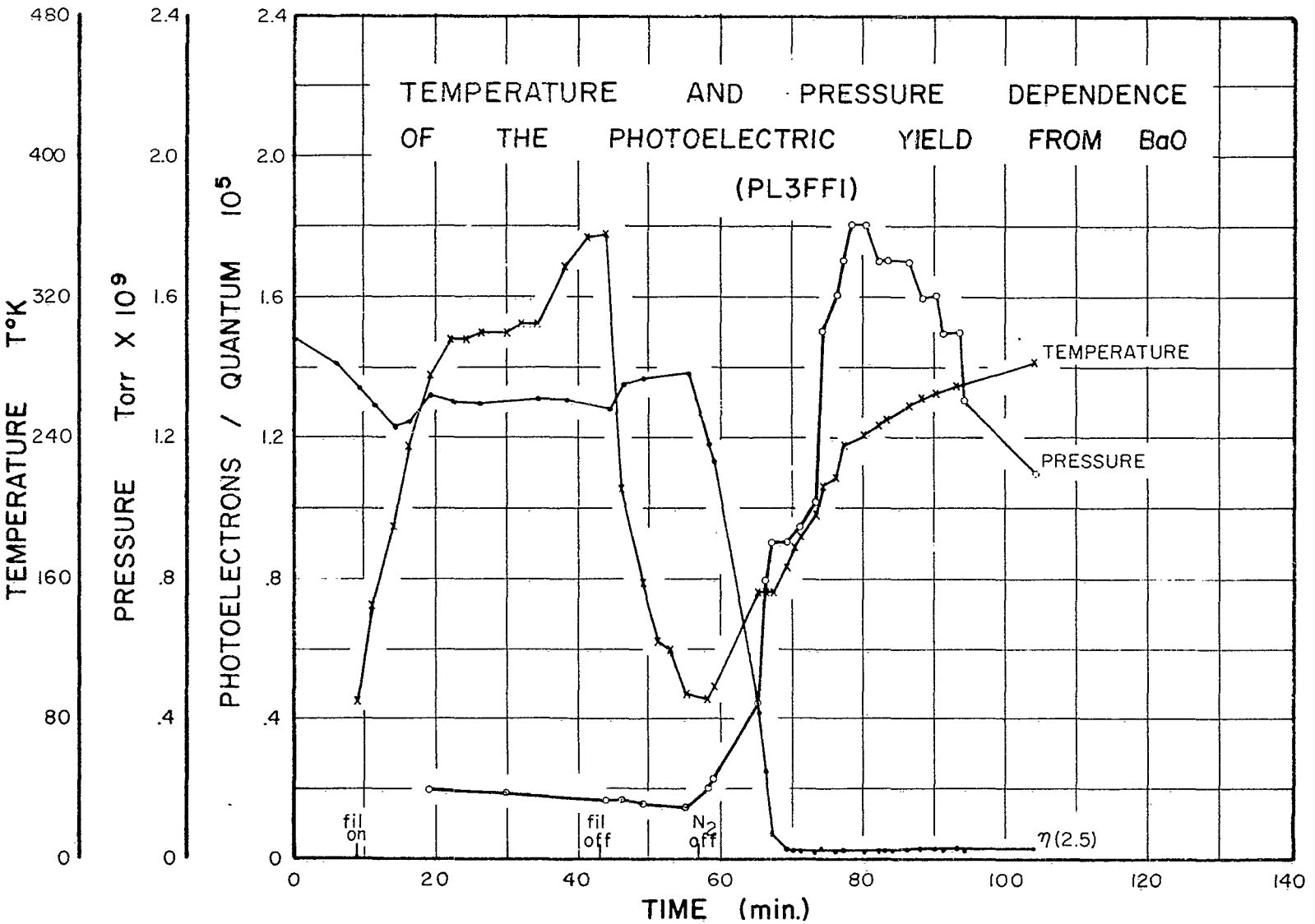
TEMPERATURE AND PRESSURE DEPENDENCE
OF THE PHOTOELECTRIC YIELD FROM BaO
(PL3FF1)
TEMPERATURE T°K
PRESSURE Torr X 10⁹
PHOTOELECTRONS / QUANTUM 10⁵
TIME (min.)
TEMPERATURE
PRESSURE
η(2.5)
fil on
fil off
N2 off
480
400
320
240
160
80
0
2.4
2.0
1.6
1.2
.8
.4
0
20
40
60
80
100
120
140

FIG. 4

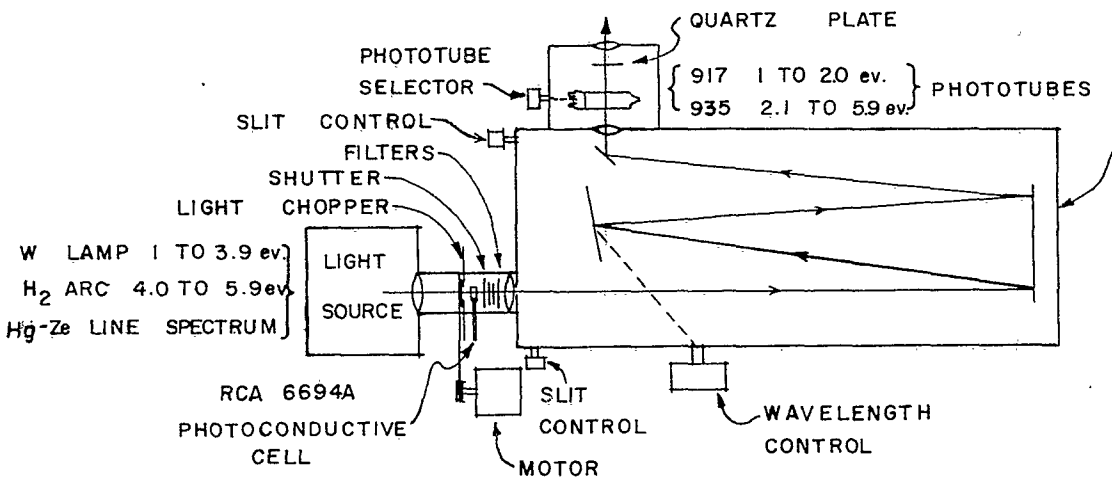

Δ ev.	5ev.	3.5ev.	2.5ev.
1.0 MM	~.07	~.03	~.02
0.5 MM	~.04	~.02	~.01

MONOCHROMATIC
LIGHT SOURCE

FIG. 5

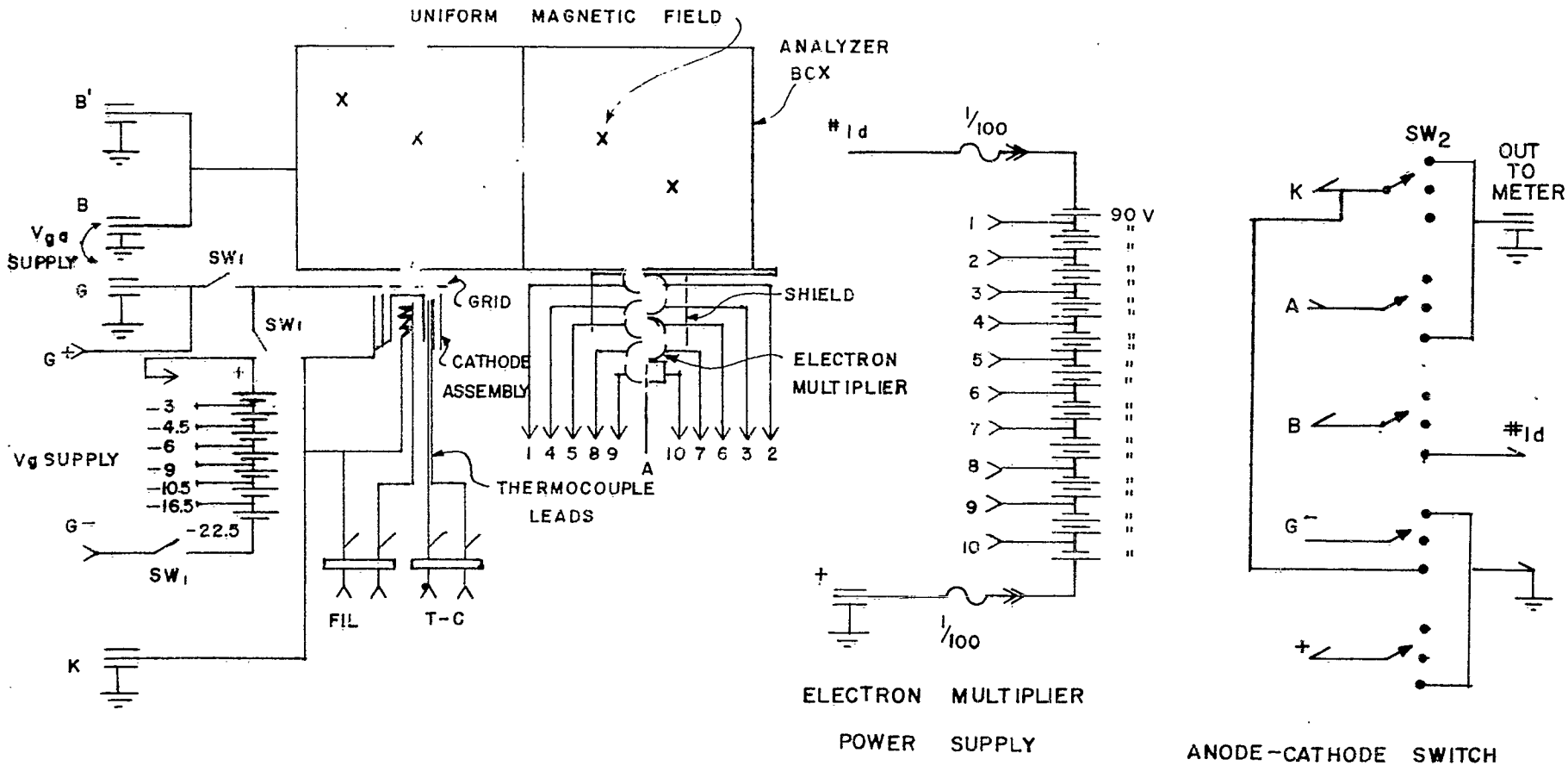

ELECTRON ENERGY ANALYZER SYSTEM

FIG. 6

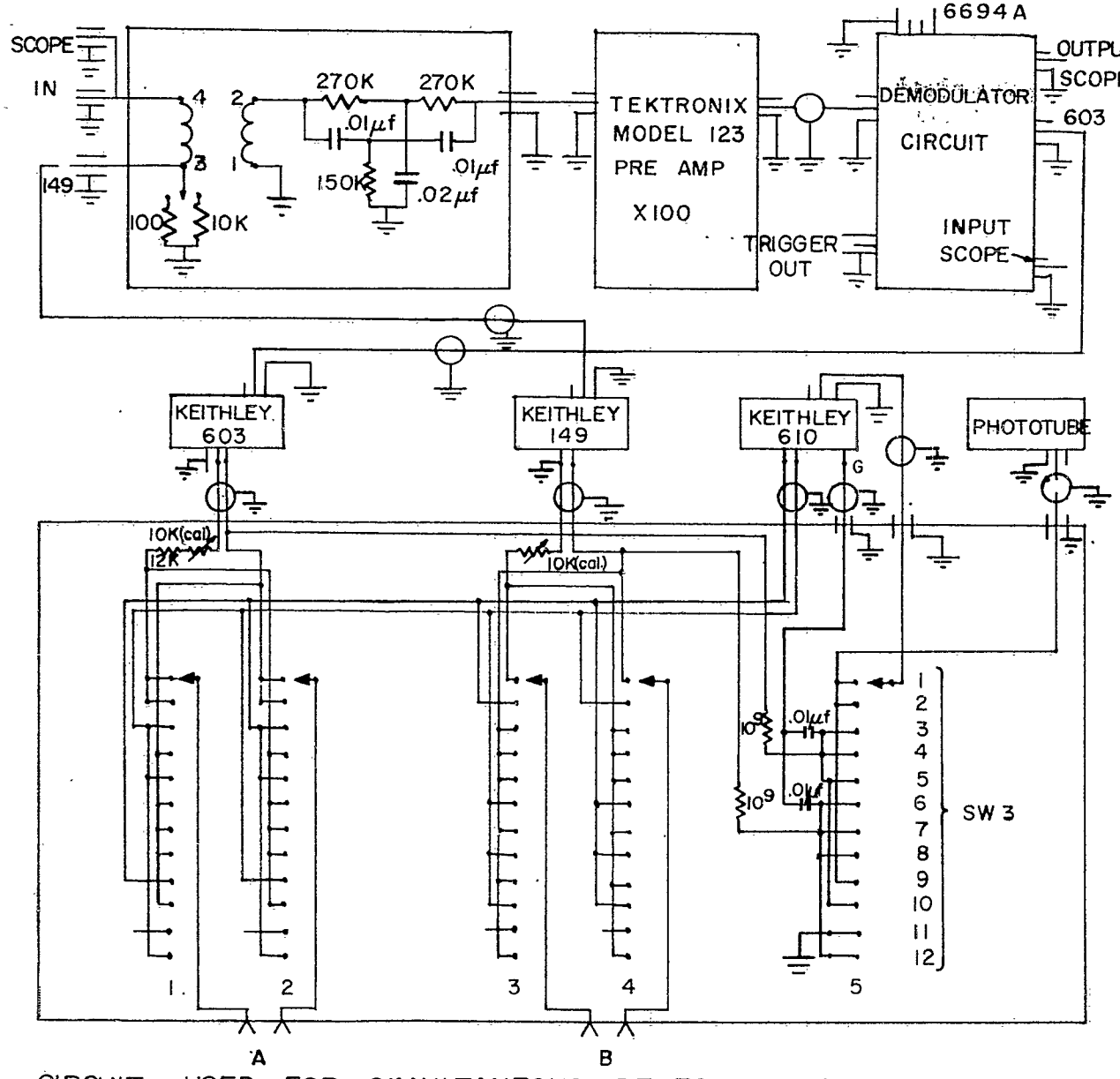

SW3 POSITION	RECORDER A	CHANNEL B	FUNCTION OF K610
1	Ip(603)	It(149)	Ipt
2	Ip(603)	Ipt(610)	Ipt
3	∫Ipd(610)	Itd(149)	∫Ipd
4	Ipd(603)	Itd(149)	∫Ipd
5	∫Ipd(610)	Itd(149)	∫Ipd
6	Ipd(603)	∫Itd(610)	∫Itd
7	Ipd(603)	Itd(149)	∫Itd
8	Ipd(603)	∫Itd(610)	∫Itd
9	Ipt(610)	Itd(149)	Ipt
10	Ipd(603)	∫Ipd(610)	∫Ipd
11	OPEN	OPEN	GRND.
12	∫Itd(610)	Itd(149)	∫Itd

Ipt→PHOTOTUBE CURRENT.

Ip→AC PHOTOEMISSION CURRENT.

It→DC THERMIONIC CURRENT.

Ipd→AC PHOTOEMISSION DISTRIBUTION CURRENT.

∫Ipd→INTEGRAL OF PHOTOEMISSION CURRENT.

Itd→DC THERMIONIC DISTRIBUTION CURRENT.

∫Itd→INTEGRAL OF THERMIONIC CURRENT.

CIRCUIT USED FOR SIMULTANEOUS DETECTION AND DISPLAY OF AC PHOTOELCTRIC EMISSION AND DC THERMIONIC EMISSION.

FIG. 7

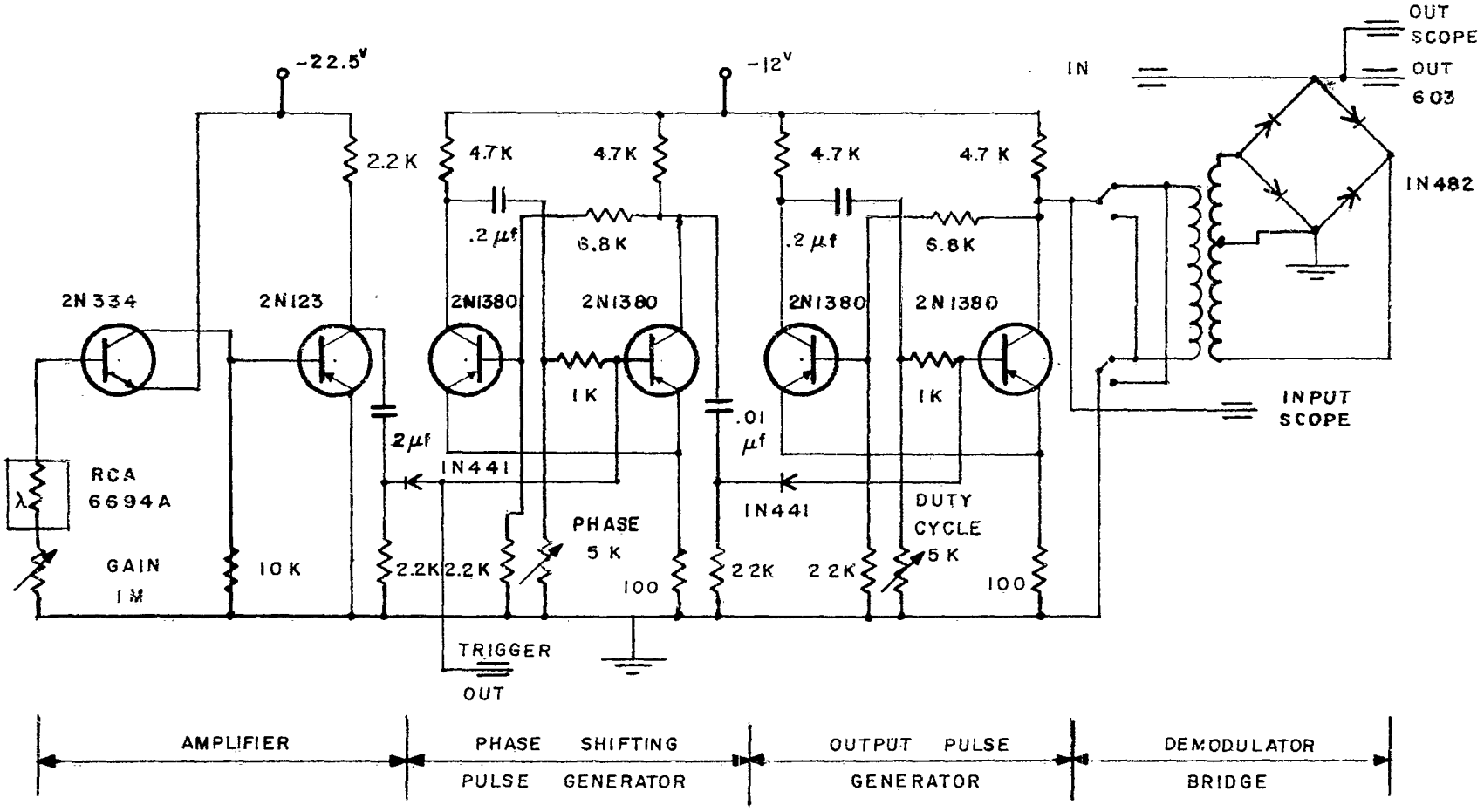

DEMODULATOR CIRCUIT

FIG. 8

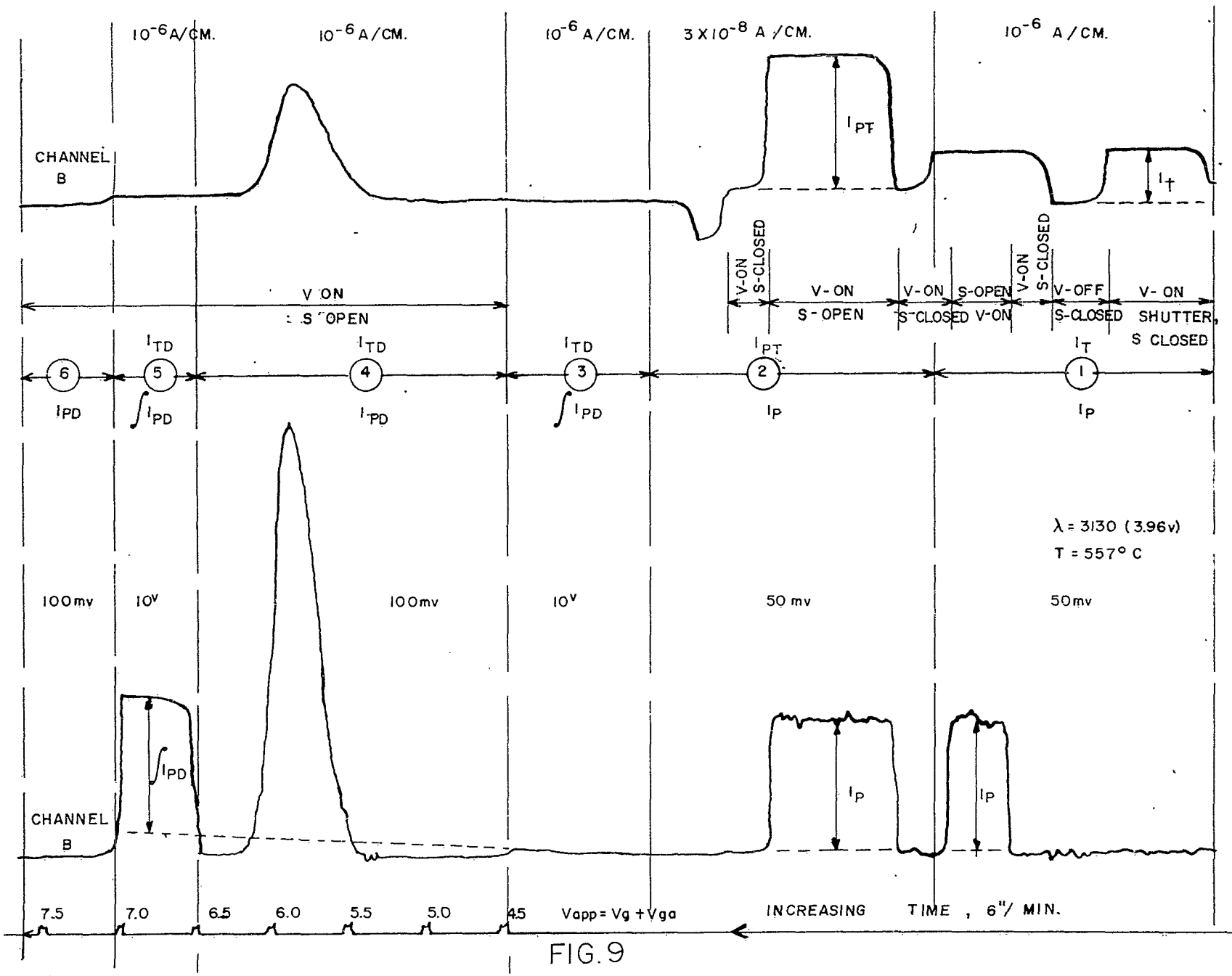
10^{-6} A/CM.
10^{-6} A/CM.
10^{-6} A/CM.
3×10^{-8} A/CM.
10^{-6} A/CM.
CHANNEL B
I_{PT}
I_T
V-ON
S-CLOSED
V-ON
S-OPEN
V-ON
S-OPEN
S-CLOSED
V-ON
V-ON
S-CLOSED
V-OFF
S-CLOSED
V-ON
SHUTTER, S CLOSED
V ON
S OPEN
I_{TD}
I_{TD}
I_{TD}
I_{PT}
I_T
6
5
4
3
2
1
I_{PD}
$\int I_{PD}$
I_{PD}
$\int I_{PD}$
I_P
I_P
λ = 3130 (3.96v)
T = 557° C
100mv
10v
100mv
10v
50 mv
50mv
$\int I_{PD}$
I_P
I_P
CHANNEL B
7.5
7.0
6.5
6.0
5.5
5.0
4.5
Vapp = Vg + Vga
INCREASING TIME , 6"/ MIN.

FIG. 9

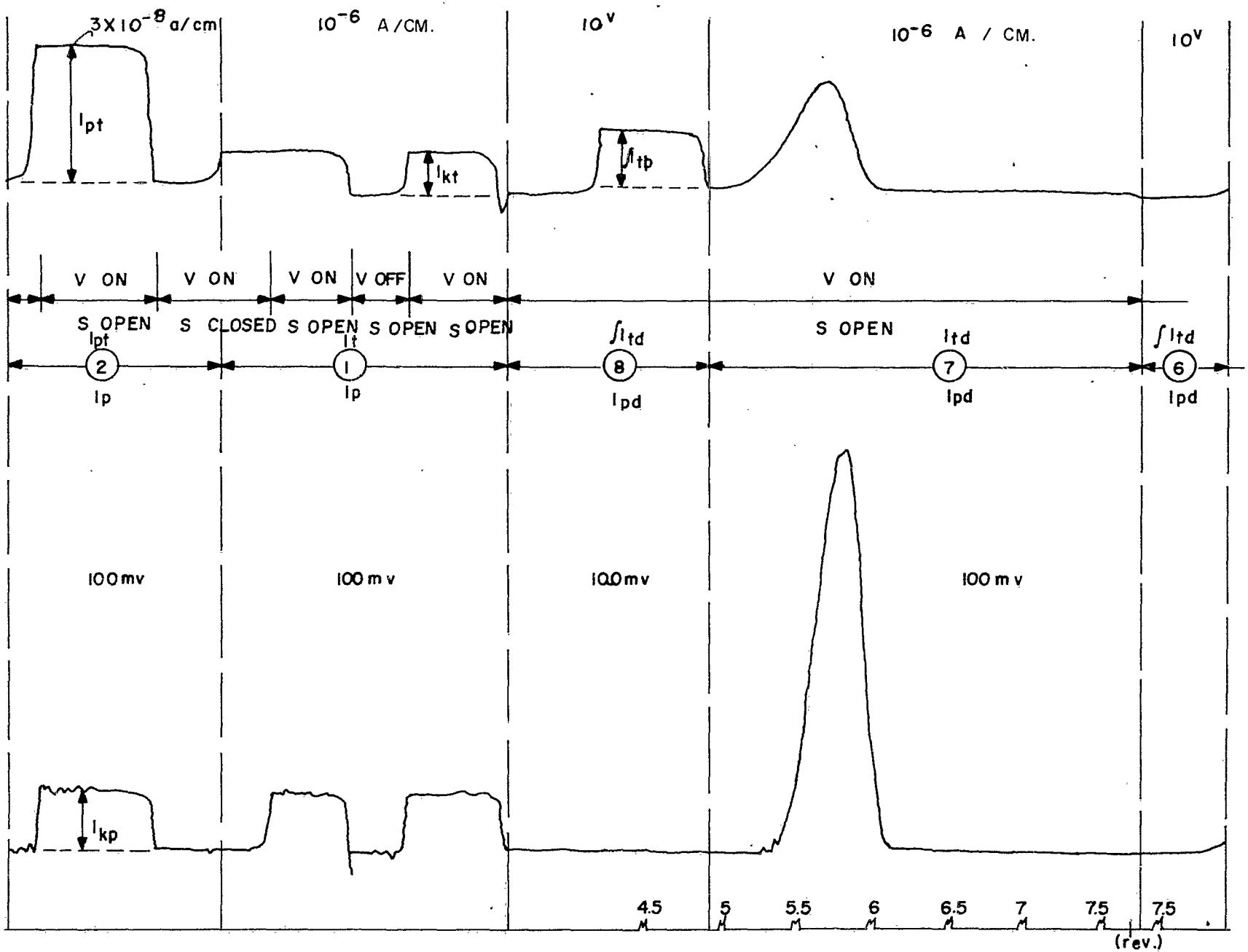
3X10⁻⁸ a/cm
10⁻⁶ A/CM.
10 V
10⁻⁶ A / CM.
10 V
Ipt
Ikt
∫Itp
V ON
V ON
V ON
V OFF
V ON
V ON
S OPEN
S CLOSED
S OPEN
S OPEN
S OPEN
S OPEN
Ipt
It
∫Itd
Itd
∫Itd
2
1
8
7
6
Ip
Ip
Ipd
Ipd
Ipd
100mv
100 mv
100mv
100 mv
Ikp
4.5
5
5.5
6
6.5
7
7.5
7.5
(rev.)

FIG.10

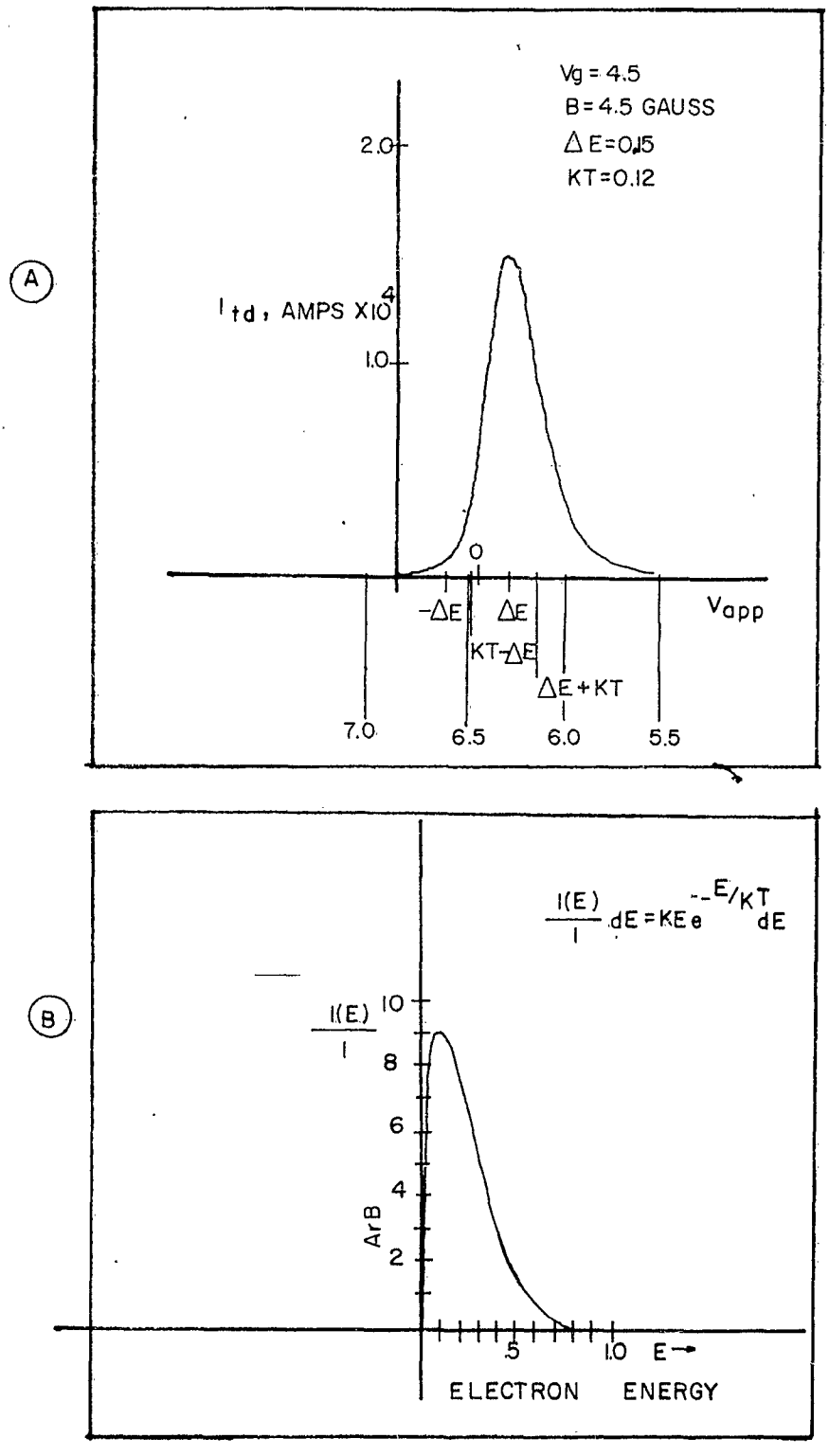

THERMIONIC EMISSION ENERGY DISTRIBUTION

FIG. 11

EVALUATION DATA FOR ENERGY ANALYZER

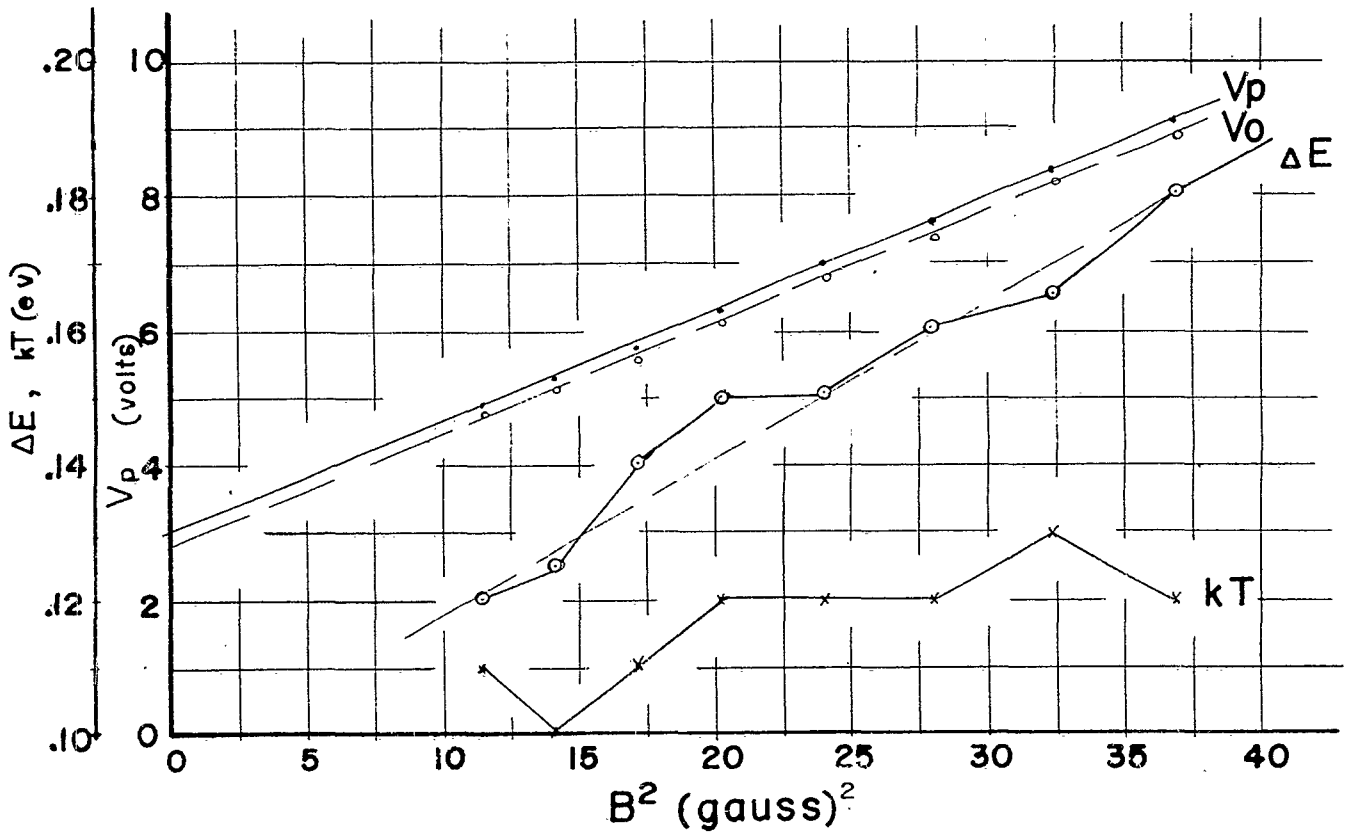

FIG. 12

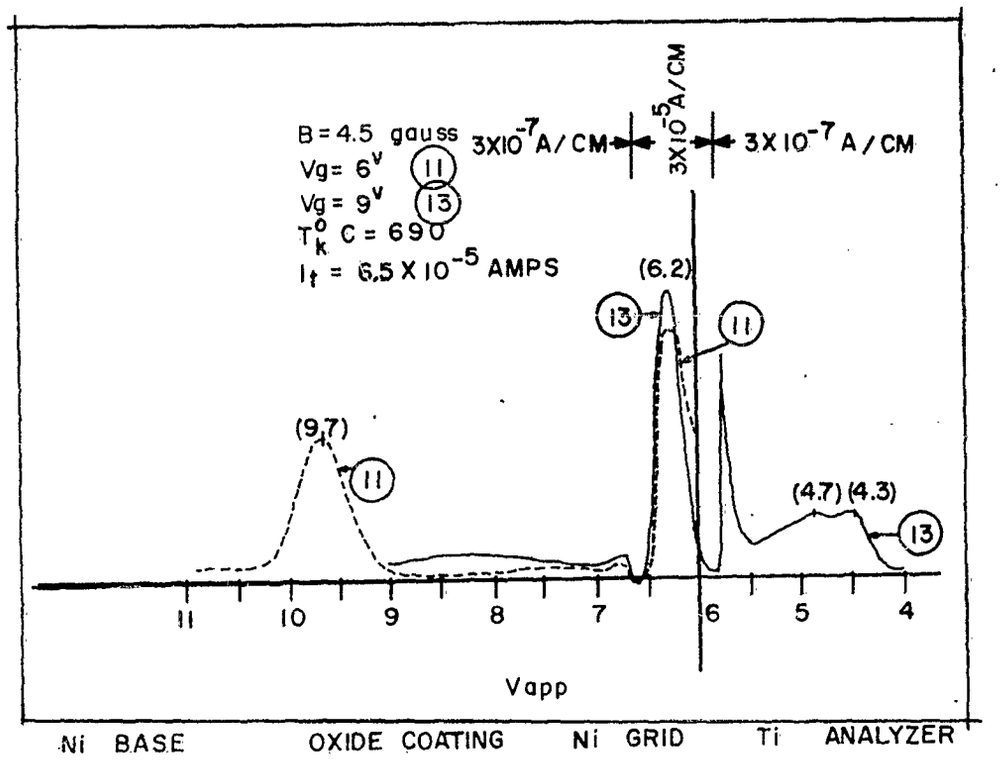

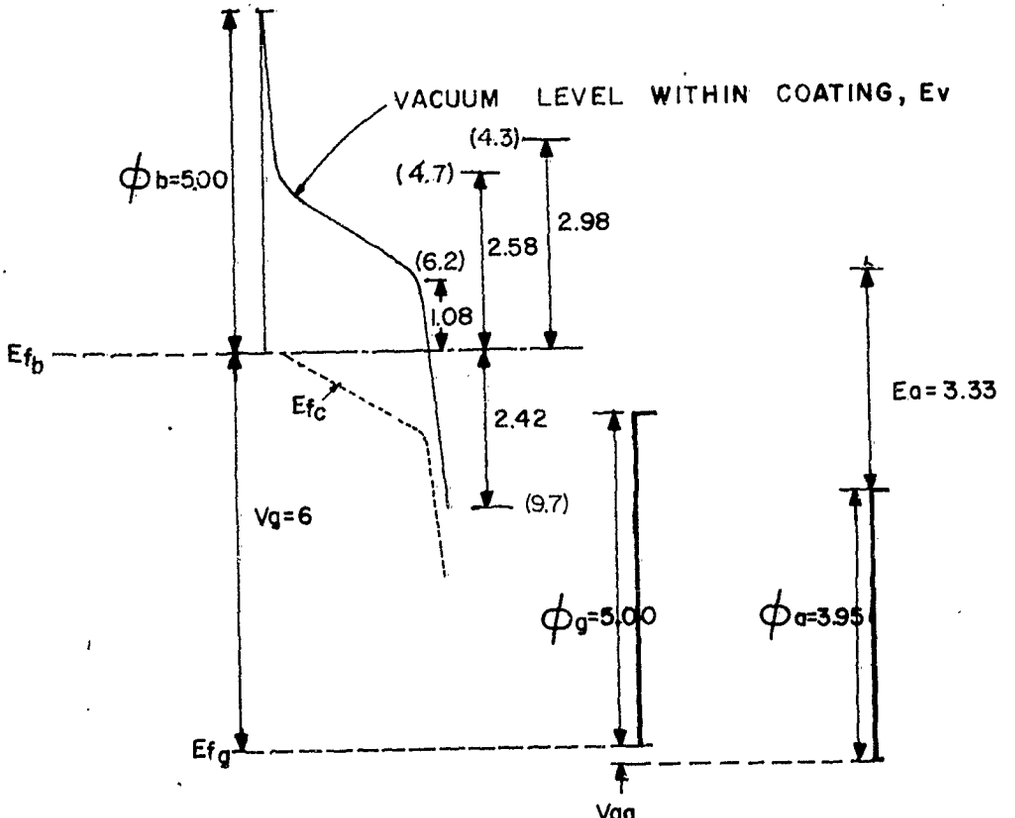

THERMIONIC EMISSION ENERGY DISTRIBUTION

FIG 13

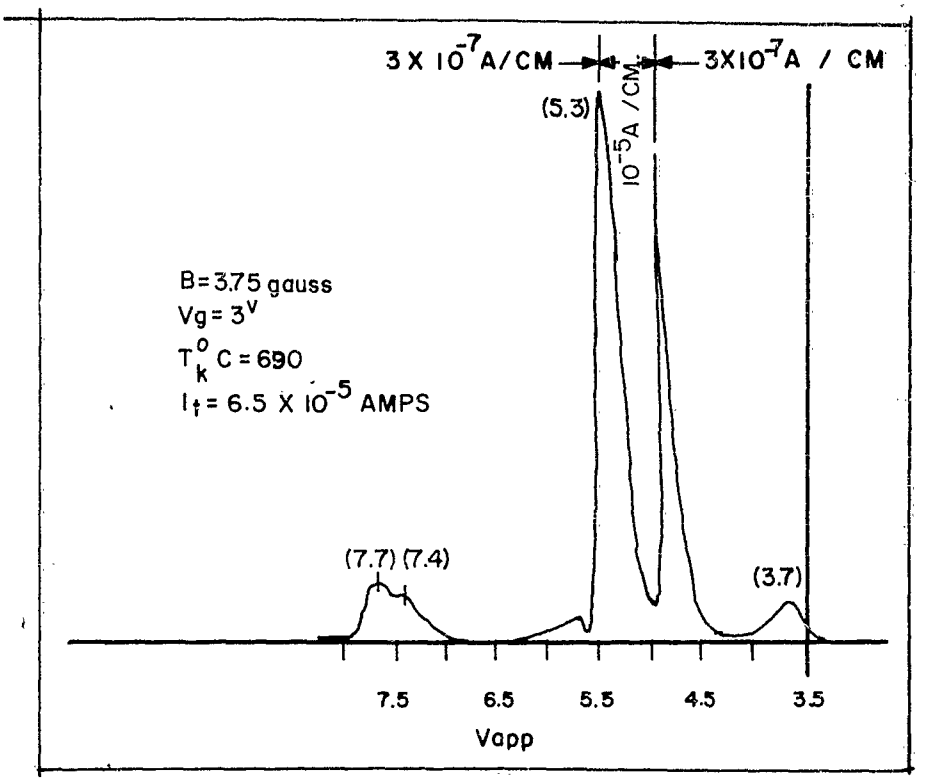

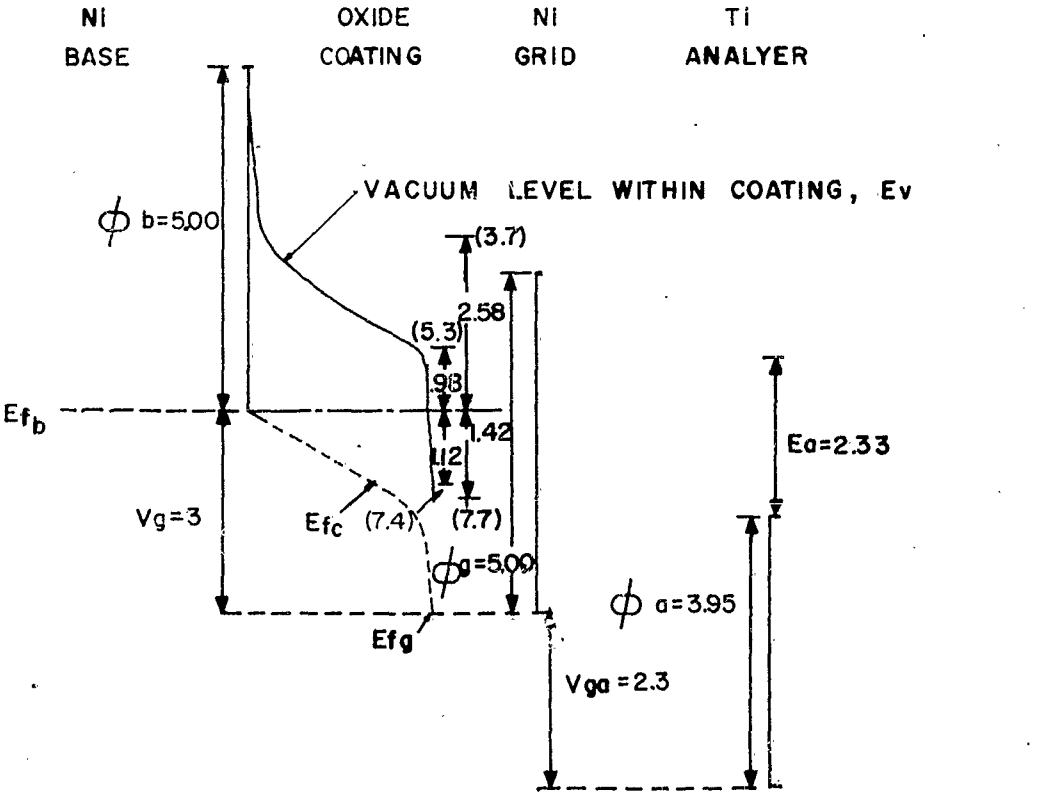

THERMIONIC EMISSION ENERGY DISTRIBUTION

FIG. 14

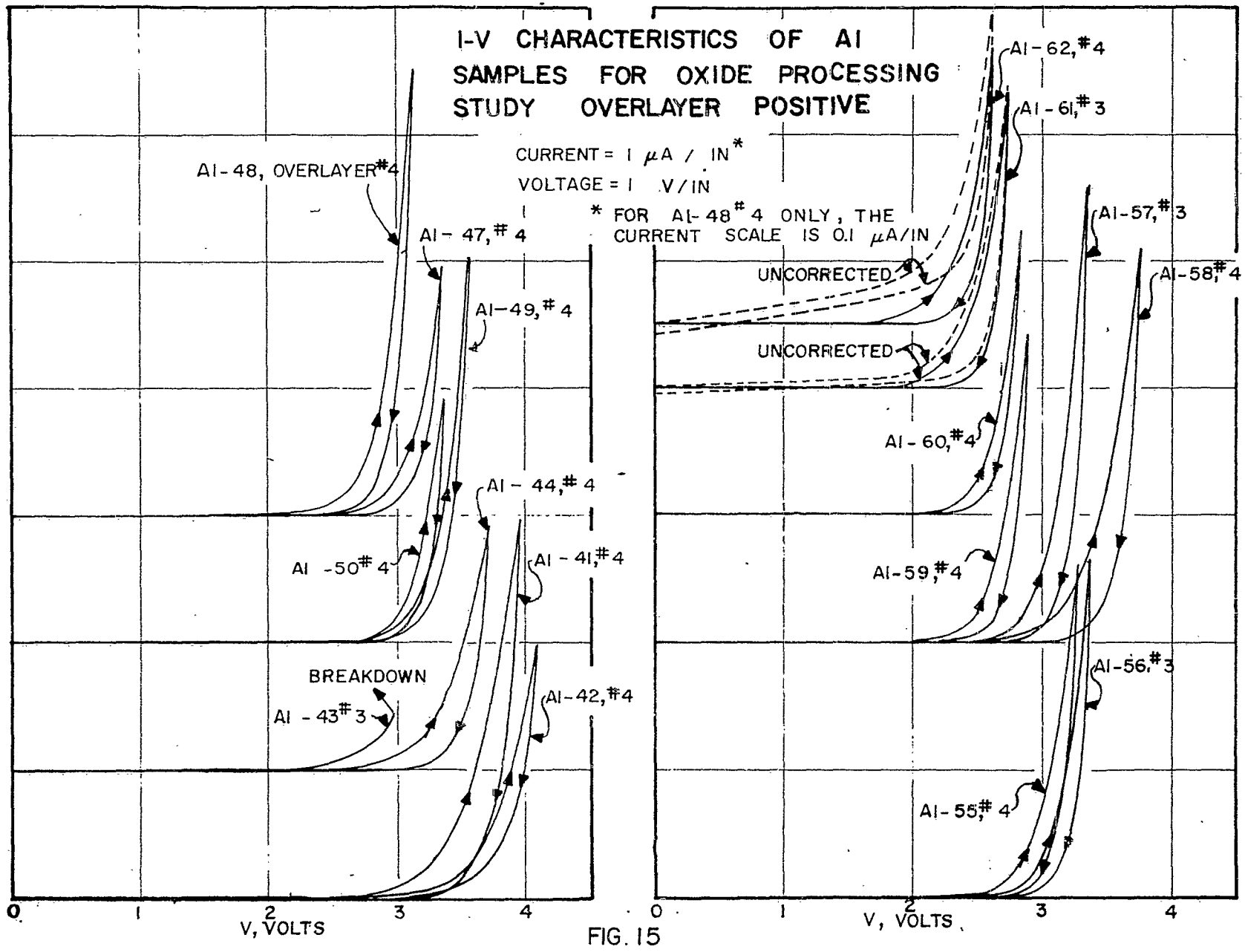
I-V CHARACTERISTICS OF Al SAMPLES FOR OXIDE PROCESSING STUDY OVERLAYER POSITIVE
CURRENT = 1 μA / IN*
VOLTAGE = 1 V/IN
* FOR Al-48 #4 ONLY, THE CURRENT SCALE IS 0.1 μA/IN
Al-48, OVERLAYER #4
Al-47, #4
Al-49, #4
Al-44, #4
Al-50 #4
Al-41, #4
BREAKDOWN
Al-43 #3
Al-42, #4
Al-62, #4
Al-61, #3
UNCORRECTED
UNCORRECTED
Al-57, #3
Al-58, #4
Al-60, #4
Al-59, #4
Al-56, #3
Al-55, #4
0
1
2
3
4
V, VOLTS
0
1
2
3
4
V, VOLTS

FIG. 15

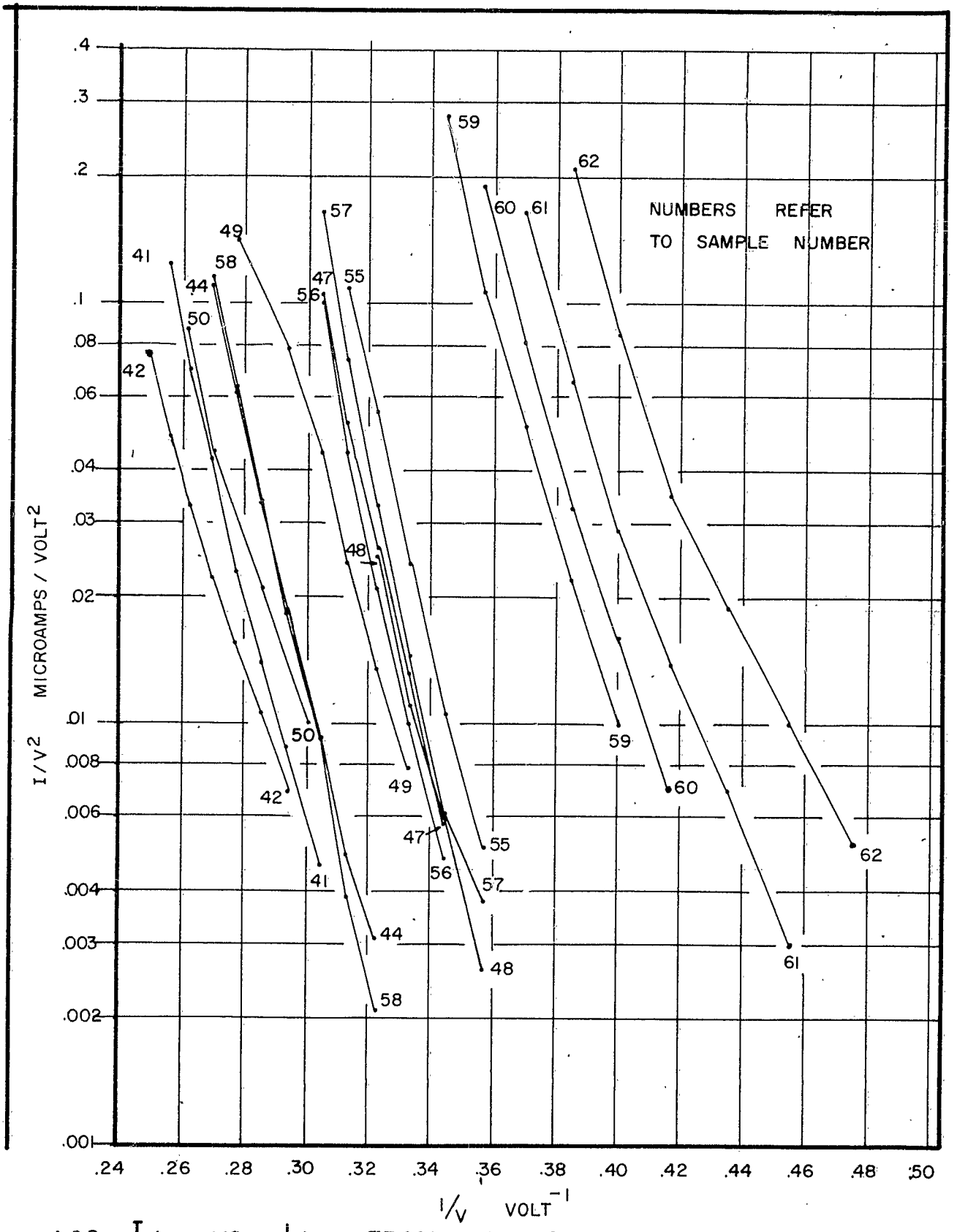

LOG I/V^2 VS. $1/V$ FROM INITIAL IV CHARACTERISTICS, VOLTAGE DECREASING

FIG. 16.

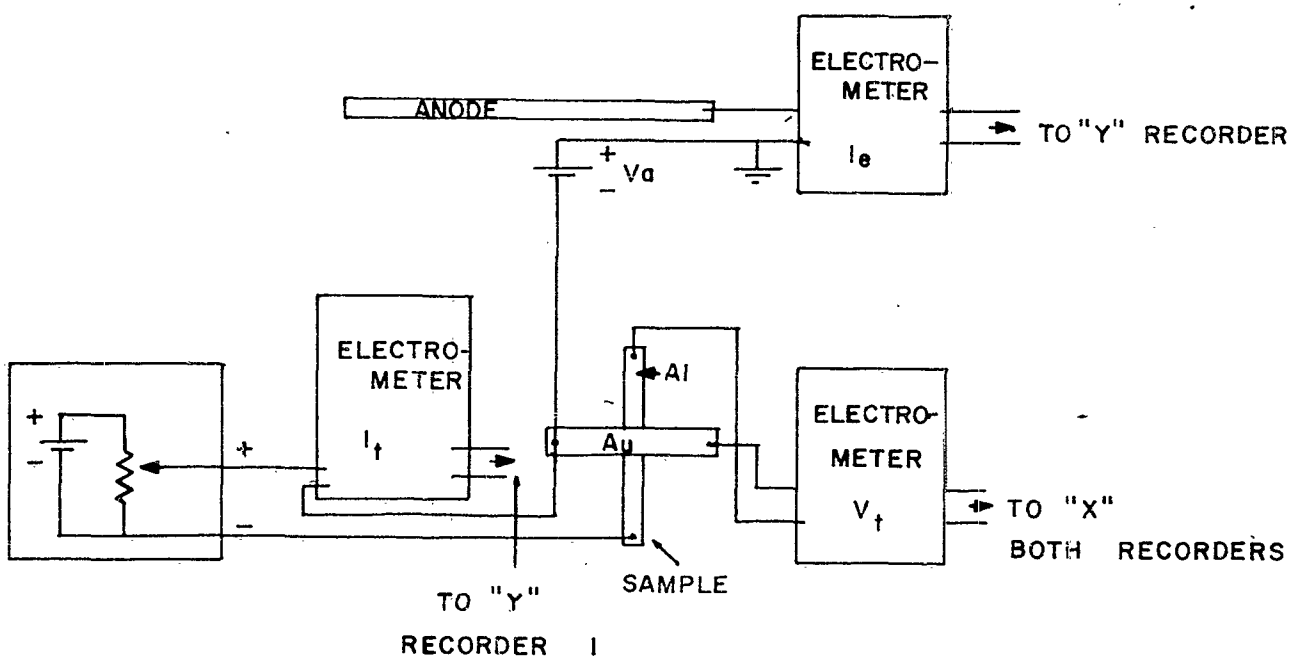

CIRCUIT USED FOR MEASURING EMISSION INTO VACUUM FROM Al-Al_2O_3-Au THIN FILM DEVICES

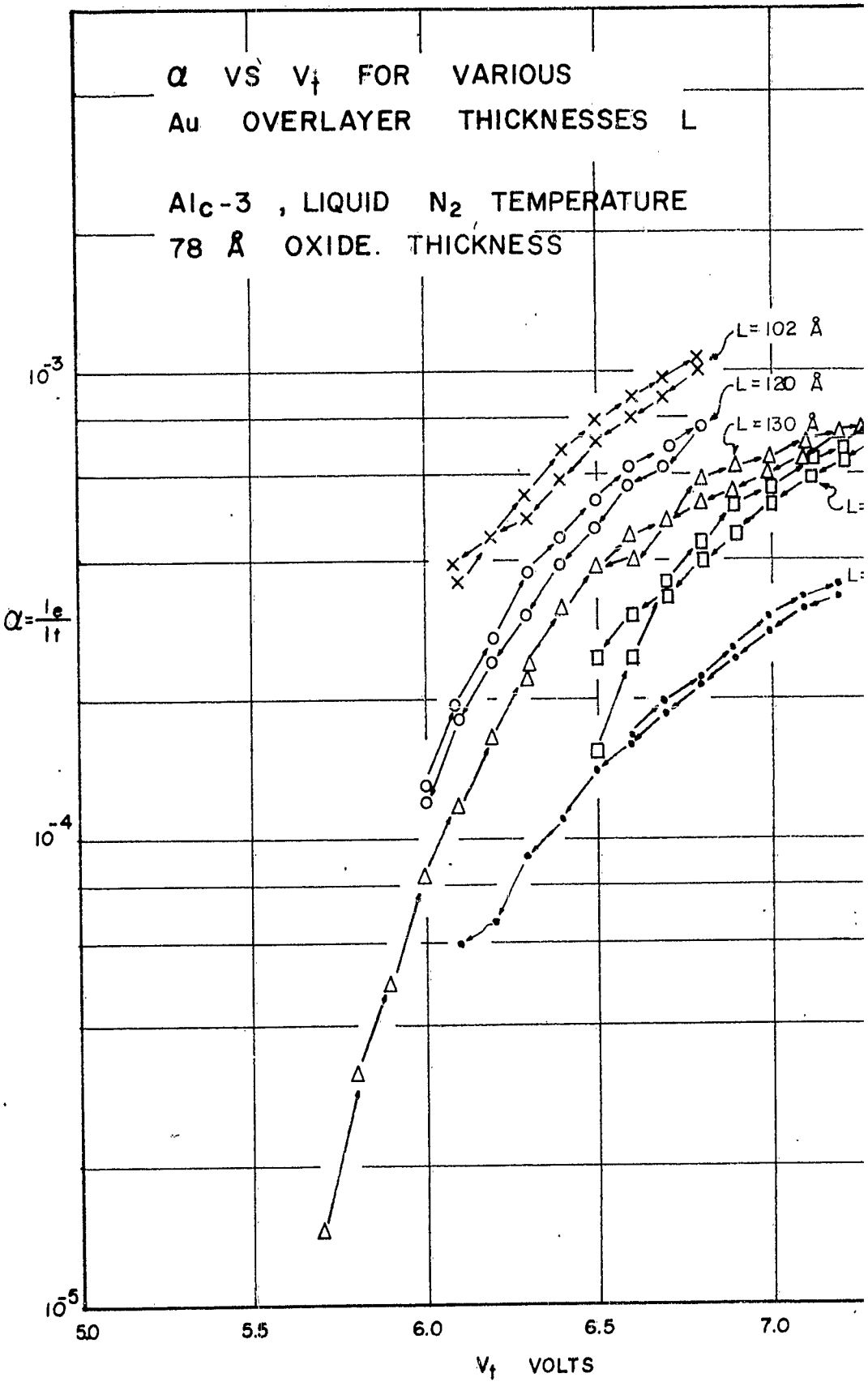
α VS V_t FOR VARIOUS
Au OVERLAYER THICKNESSES L
$Alc-3$, LIQUID N_2 TEMPERATURE
78 Å OXIDE. THICKNESS
L= 102 Å
L= 120 Å
L= 130 Å
10^{-3}
10^{-4}
10^{-5}
$\alpha = \frac{I_e}{I_t}$
5.0
5.5
6.0
6.5
7.0
V_t VOLTS

FIG. 18

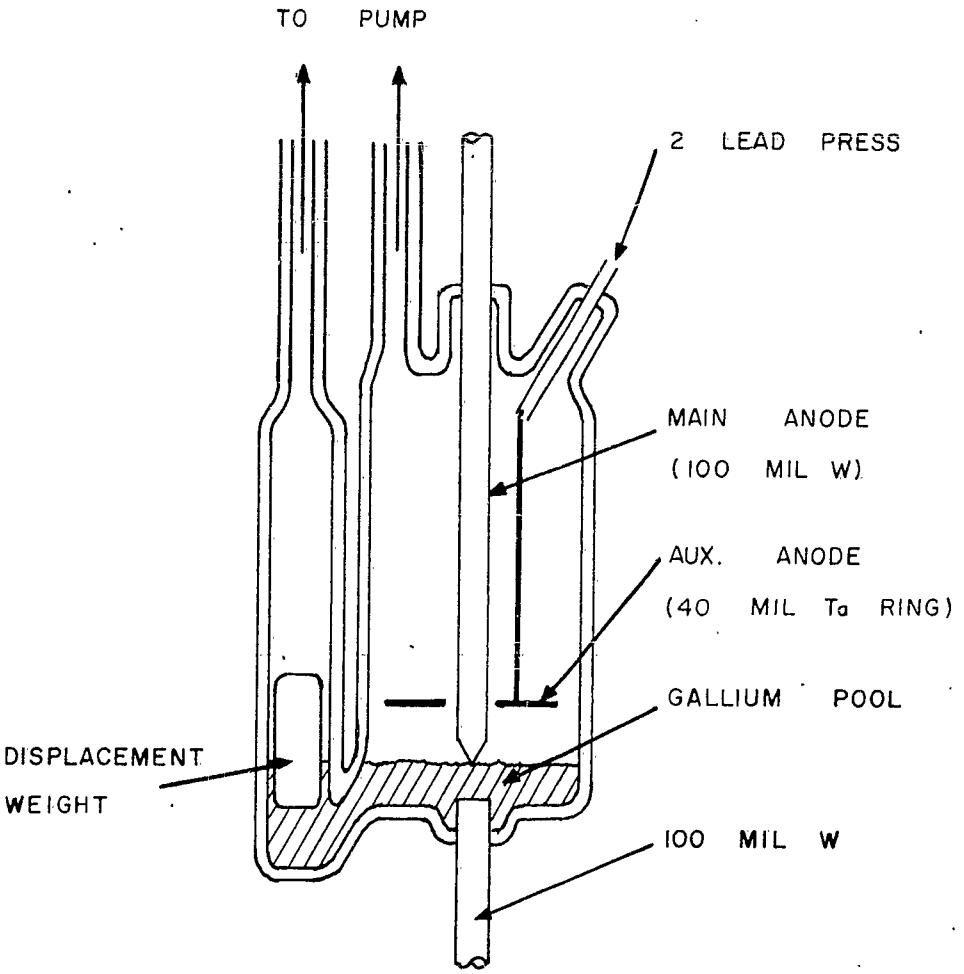

STRUCTURE USED IN GA POOL ARC DISCHARGE STUDIES

FIG. 19

Air Force Cambridge Research Laboratories, Office of Aerospace Research-Laurence G. Hanscom Field, Bedford, Massachusetts.
Rpt Nr AFCRL-63-84, STUDIES OF PRIMARY ELECTRON SOURCES: Scientific Report No. 6, March 1963, 57 pp. illus., 7 refs.

Unclassified Report

A structure designed to expose an oxide cathode to a controlled Ba or Sr pressure is described and results are presented. Simultaneous determination of photoelectric and thermionic emission energy distribution measurements from BaO are used in an evaluation of the analyzer system. A measure of the potential profile in a cathode undercurrent drain conditions is derived.

Methods of formation of Al_2O_3 films for thin film tunnel current devices are compared; the electrical properties of the insulating films are shown to be insensitive to the anodizing techniques used. Preliminary measurements of electron emission from $Al-Al_2O_3-Au$ devices are presented. Arc formation above a liquid gallium pool cathode is discussed and possible switching applications are suggested.

(over)

Unclassified

1. Cathodes (Electron Tubes)
2. Cold Cathode Tubes
3. Field Emission
4. Oxide Cathodes
5. Thermionic Emission
6. Thin Films

I. Project 4619 Task 46190
II. Contract AF 19(604)-8381
III. Electron Tube Research Laboratory, University of Minnesota Institute of Technology
IV. Prepared by D.E.Anderson